Catena 220 (2023) 106724

Contents lists available at ScienceDirect

Catena

journal homepage: www.elsevier.com/locate/catena

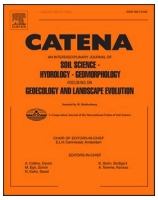

Multiproxy approach to the reconstruction of soil denudation events and the disappearance of Luvisols in the loess landscape of south-western Poland

Aleksandra Loba [a,b,*], Junjie Zhang [c], Sumiko Tsukamoto [c], Marek Kasprzak [d], Joanna Beata Kowalska [b], Manfred Frechen [c], Jarosław Waroszewski [b]

[a] Nicolaus Copernicus University in Toruń, Faculty of Earth Sciences and Spatial Management, Lwowska 1, 87-100, Toruń, Poland
[b] Wrocław University of Environmental and Life Sciences, Institute of Soil Science, Plant Nutrition and Environmental Protection, Grunwaldzka 53, 50-357 Wrocław, Poland
[c] Leibniz Institute for Applied Geophysics (LIAG), Stilleweg 2, 30655 Hannover, Germany
[d] University of Wroclaw, Institute of Geography and Regional Development, Plac Uniwersytecki 1, 50-137 Wrocław, Poland

ARTICLE INFO

Keywords:
Loess
Soil erosion
Denudation
OSL dating
Soil micromorphology
ERT
Luvisols

ABSTRACT

Loess landscapes are highly susceptible to soil redeposition processes and thus may provide detailed insights into the record of denudation processes. Using optically stimulated luminescence dating and the soil micromorphology of 12 soil profiles, we reconstructed a complete record of denudation processes in south-western Poland. The first episode of soil redeposition took place around 9.1 ka. The denudation events that followed were attributed to the Neolithic (6.4 ± 0.3 ka), early Bronze Age (3.8 ± 0.2 ka), early and late Middle Ages (1.5 ± 0.1 ka and 0.7 ± 0.03 ka, respectively) and early Modern (0.4 ± 0.02 ka). As a consequence of the denudation processes, the soil cover in the studied area had been strongly reshaped. The predominant Luvisols had experienced progressive erosion processes that led first to a significant shallowing of the eluvial and argic horizons (truncated Luvisol) and, after some time, to their complete removal. Further thinning of the loess mantles had exposed geological substrates with very weak pedogenic alternations, thus pushing their transformation towards Regosol types. Similarly, Regosols occurred in toeslopes where freshly eroded material had been deposited, and where diagnostic horizons had not yet developed. Modern soil erosion rates in the studied loess area have considerably increased, and it is estimated that the Luvisol status may be completely transformed within approximately 80–300 years, if not sooner, due to progressive climate change.

1. Introduction

Denudation processes understood as a surface lowering of the land by erosion and near-surface processes, lead to a significant landscape modifications (Karasiewicz et al., 2014; Raab et al., 2021). In agricultural landscapes and hill county, the soil erosion is essential for denudation (Meij et al., 2019; Raab et al., 2018). Erosion processes disintegrate and remove topsoil from the upslope and deposit the transported material in the toe slope, where it forms colluvial soils. Thus, as a consequence irreversible changes occur in the natural structure, physical, chemical and morphological features of these soils and their corresponding horizons as well as their distribution in the landscape (Kaiser et al., 2021; Matecka and Świtoniak, 2020; Pindral and Świtoniak, 2017; Zádorová et al., 2014; Zádorová and Penížek, 2018).

One of the materials most susceptible to denudation processes is loess (Poręba et al., 2019; Šimanský et al., 2019; Zhang et al., 2018b), sediment that is widespread on a global scale (Muhs, 2013). In Europe, loess deposits occur from France to Ukraine and Russia (Haase et al., 2007; Lehmkuhl et al., 2021; Scheib et al., 2014) with their most intense accumulation having occurred during the Last Glacial Maximum (LGM) in Marine Isotope Stage (MIS) 2 (Frechen, 2003; Jary, 1996). Since the Neolithic, soil erosion/deposition processes have been accelerated in the loess-covered areas due to deforestation and the use of that land for arable (Altermann et al., 2005; Gerlach et al., 2012; Kołodyńska-Gawrysiak et al., 2017). These changes in land use occurred because most fertile soils, such as Chernozems and Pheozems, characterised by a

* Corresponding author at: Nicolaus Copernicus University in Toruń, Faculty of Earth Sciences and Spatial Management, Lwowska 1, 87-100, Toruń, Poland.
E-mail address: aleloba@umk.pl (A. Loba).

https://doi.org/10.1016/j.catena.2022.106724
Received 6 May 2022; Received in revised form 10 October 2022; Accepted 15 October 2022
Available online 24 October 2022

thick, dark humus (chernic/mollic) horizon, have developed in loess belts (Altermann et al., 2005; Drewnik et al., 2014; Gerlach et al., 2012; Labaz et al., 2018; Smetanová et al., 2017).

Much has been written about erosion and redeposition processes in soils bearing chernic (and mollic) horizons developed in loess-dominated landscapes in the Czech Republic (Smetanová et al., 2017; Zádorová et al., 2011), Germany (Altermann et al., 2005; Gerlach et al., 2012), Poland (Drewnik and Żyła, 2019; Kabała et al., 2019), Ukraine (Dreibrodt et al., 2022; Łanczont et al., 2021) and Russia (Khokhlova et al., 2015). Erosion processes thin humus-rich horizons and, as a result, their colour is greatly lightened (Drewnik and Żyła, 2019). Consequently, the criteria for chernic/mollic horizons are not met and the soils are transformed into Luvisols (Kabała et al., 2019; Labaz et al., 2018). These are still fertile soils because of their high saturation with alkaline cations and favourable hydro-physical properties (Glina et al., 2014; Rejman et al., 2014a; Turski and Witkowska-Walczak, 2004; Vitharana et al., 2008). However, they are intensively used in agriculture and thus exposed to further degradation (Klimowicz and Uziak, 2001). Erosion and soil degradation are issues specifically highlighted in the European Parliament's resolution on soil protection from 2021 (European Parliament, 2021) and the Food and Agriculture Organization's (FAO) statement of 2019 (FAO, 2019). Thus, detailed actual research on this topic is still needed.

Using knowledge on soil erosion rates, soil conservation practices can be optimised (Alewell et al., 2017). Erosion processes have been widely studied in loess landscapes using isotope techniques, such as beryllium-10, cesium-137, plutonium-239/240, excess lead-210, $\delta^{13}C$, $\delta^{15}N$, and classical methods, including closed depressions and the Universal Soil Loss Equation, in France, Germany, Belgium, Poland, China and the USA (Baumgart et al., 2017; Dreibrodt et al., 2013, 2010b; Gillijns et al., 2005; Jagercikova et al., 2015, 2014; Jakab et al., 2018; Kołodyńska-Gawrysiak et al., 2018; Li et al., 2005; Liu et al., 2018; Loba et al., 2022, 2021; Poręba et al., 2019, 2015; Tuo et al., 2018; Van Oost et al., 2003; Yu et al., 2017; Zhang et al., 2018a; Zhang et al., 2019). The data obtained on soil erosion may be supported by dating techniques, such as radiocarbon (^{14}C) dating of soil organic matter, charcoals from colluvial sediments or optically stimulated luminescence (OSL), which can provide information concerning when the constituent mineral grains were last exposed to sunlight, thus providing an age for the sediment (re) deposition (Fuchs et al., 2010; Kołodyńska-Gawrysiak et al., 2017; Novák et al., 2018; Poręba et al., 2011; Rahimzadeh et al., 2019; Zgłobicki and Rodzik, 2007). Such approaches enable the reconstruction of erosion–deposition events, an analysis of the evolution of relief in the Pleistocene and Holocene, and the modelling of past environmental dynamics (Döhler et al., 2018; Kołodyńska-Gawrysiak et al., 2018; Malik et al., 2021; Poręba et al., 2019; Rahimzadeh et al., 2019; Scherer et al., 2021).

Recent studies have shown that progressive climate change and agricultural intensification accelerate erosion processes (Kopittke et al., 2019; Kundzewicz and Matczak, 2012; Loba et al., 2021; Radziuk and Świtoniak, 2021; Routschek et al., 2014; Zollinger et al., 2015), and therefore the status of Luvisols occurring in the loess landscapes is uncertain. In order to track past and present changes in Luvisols we aimed to: i) reconstruct time-intervals of denudation processes using OSL dating; ii) outline the soil development trajectories forced by denudation processes; and iii) calculate the approximate timing of the disappearance of the Luvisols.

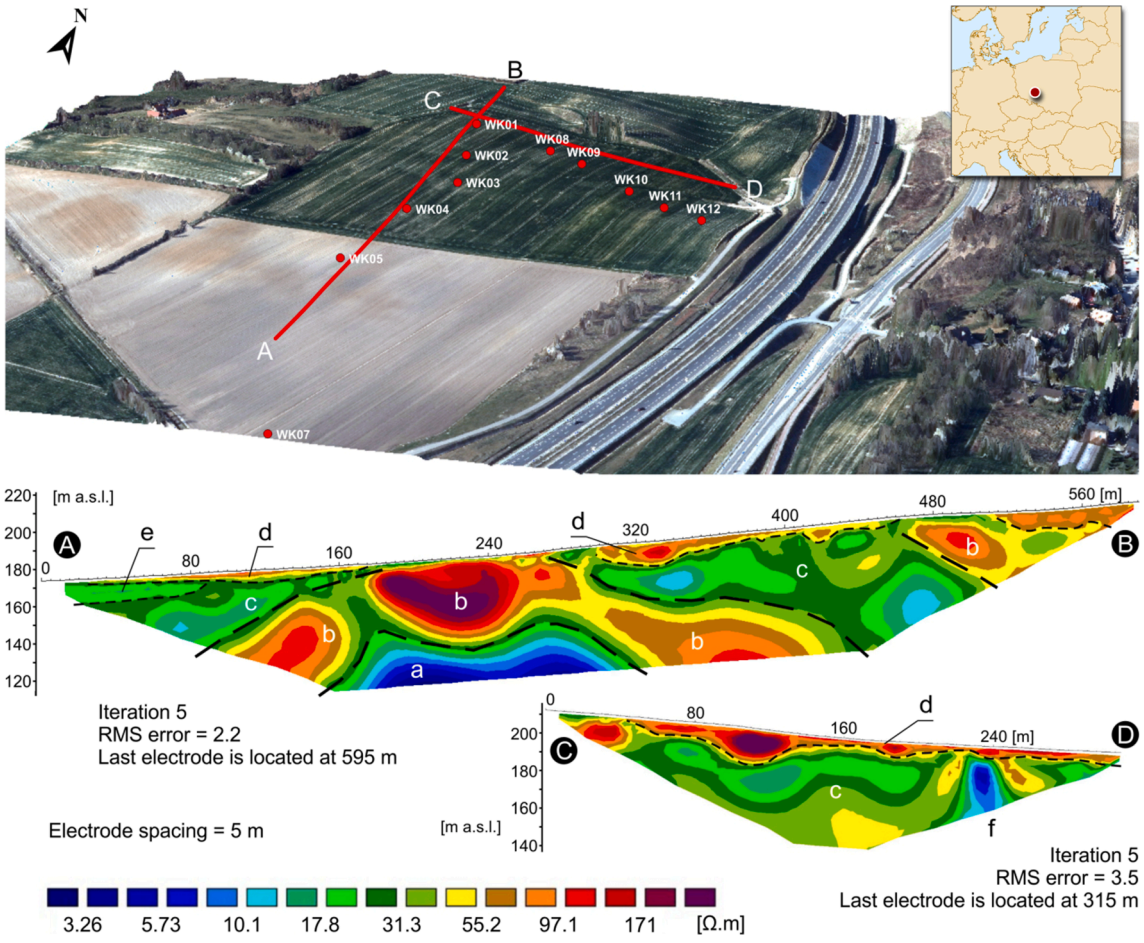

Fig. 1. Study sites in the Trzebnica Hills and inversion models for two Electrical Resistivity Tomography sections.

2. Methods

2.1. Study area and sampling strategy

The study area was situated in south-western Poland, around the edges of the Trzebnica Hills, north of Wrocław (Fig. 1, Table 1). The local lithology is dominated by Quaternary deposits, including glacial tills, fluvioglacial sediments and loess, the latter being the youngest (late Pleistocene) deposit, which is spread over the hills, forming a mantle with varying thickness (Glina et al., 2014; Jary, 1996). Most of the land is used for agriculture due to the presence of productive soils (Luvisols, Pheozems, Chernozems) (Anioł-Kwiatkowska, 1998). The study area is characterised by warm summers and a humid, continental climate. The mean annual temperature is 9.5 °C, while the mean annual precipitation ranges from 500 to 620 mm (Bac and Rojek, 2012).

Two soil transects were arranged along slopes that bore visible features of erosion and accumulation processes. Profile WK1 was a common point for both transects (Fig. 1), with the first transect including Profiles WK1–WK7, and the second WK1 and WK8–WK12. Drilling down to 70 cm between the soil profiles was done in order to assess the thickness of the loess mantle and the disappearance of the E and Bt horizons. All soil profiles were described according to the Guidelines for Soil Description (FAO, 2006) and classified according to the FAO–World Reference Base (WRB) system (IUSS Working Group WRB, 2022). From all designated soil horizons, about 1 kg of bulk material was sampled for chemical and physical analysis. Additionally, 15 samples were taken for OSL dating from selected horizons by hammering steel tubes into the freshly cleaned outcrop walls, with 12 undisturbed samples being taken for micromorphological investigation using Kubiena boxes (6 × 4 cm).

2.2. Electrical resistivity tomography

The ERT measurements allow for a visualisation of the variability of the geological structure of the shallow ground and distinction of the main lithological units (Fig. 1). Electrical resistivity tomography (ERT) was carried out as part of the fieldwork (Kasprzak and Traczyk, 2014), and included zones of previously made soil profiles and drillings. The survey campaign took place in rain-free weather conditions and on moist, vegetation-free soil. An ARES II device, with a set of cables enabling the simultaneous connection of 80 electrodes distributed along the measured section, was used to perform the measurements. The measurements were taken in two sections, one 595 m long (Section AB), using rolling cables, and the other 315 m long (Section CD), and reached a maximum depth of about 75 m. In both cases, the distance between the electrodes was 5 m. This was also the resolution of the data obtained from the near-surface layer, whereas, in the deeper part of the profile, the resolution decreased. The measurements were made using the Schlumberger method—regarded as relatively universal for recognizing both vertical and horizontal structures in the subsurface—which also offers a relatively large number of combinations of electrodes and thus measurement points (Reynolds, 2011). The data were subjected to a smooth type of inversion (L2) using RES2DINV software (Geotomo, Malaysia), which included a topographic correction. Results are presented for the fifth iteration, with the colour scale unified for both inversion models. The interpretation of the obtained models was based on data from available geological sources (Krzyszkowski and Łabno, 2002; Winnicki, 1997), including a geological map with explanatory notes (Winnicki, 1990, 1985) and nearby boreholes data (Central Geological Database).

2.3. Soil micromorphology

Sampled soil blocks were left to air-dry. They were then embedded in polyester resin (T.R.A., Finress) and left to cure for 2–4 weeks at room temperature, after which, 1–2-cm-thick slabs were cut from the blocks and trimmed to match the dimensions of a glass slide. The cut side of the embedded block was polished using diamond paste. The grinding and polishing on a diamond wheel were performed manually and checked regularly under the microscope until quartz interference colours matching a 30-μm-thick thin section were obtained. The thin sections were prepared at the University of Ghent (Laboratory for Mineralogy and Petrology). The thin sections were observed in both plane and polarised light using a Zeiss Axio Lab A1 transmitting-light microscope and were described according to the terminology of Stoops (Stoops, 2003).

2.4. Particle size distribution

The particle size distributions between 0.4 and 2000 μ m were measured following sample dispersion for 12 h on a rotator using 1%

Table 1
Main characteristics of studied sites.

Soil profile	Latitude and longitude	Elevation (m asl)	Inclination (°)	Slope position	Land use	Classification according to WRB (IUSS, 2022)	Horizons layout
WK1	51° 16′ 09.0″ N 17° 02′ 36.7″ E	206.8	4	Top slope	Arable land	Albic Luvisol (Aric, Cutanic, Ochric, Siltic)	Ap – AE – E – EBtg – Btg1 – Btg2
WK2	51° 16′ 06.3″ N 17° 02′ 38.3″ E	198.2	10	Shoulder	Arable land	Haplic Luvisol (Aric, Cutanic, Endodensic, Endoloamic, Ochric, Episiltic, Raptic)	Ap – A/Bt – Bt/BC – BC1 – BC2 – 2Btb – 2Bt/2BCb
WK3	51° 16′ 02.6″ N 17° 02′ 37.6″ E	191.8	13	Shoulder	Arable land	Lamellic Luvisol (Aric, Cutanic, Ochric, Siltic)	Ap – AE – Bt1 -Bt2 – BC
WK4	51° 15′ 59.3″ N 17° 02′ 37.4″ E	187.1	10	Back slope	Arable land	Stagnic Albic Luvisol (Aric, Cutanic, Ochric, Siltic)	Ap – AE – E – Ebt – Bt/E – Bt -BC
WK5	51° 15′ 56.6″ N 17° 02′ 38.5″ E	181.1	5	Back slope	Arable land	Albic Luvisol (Aric, Cutanic, Ochric, Siltic)	Ap -AEg – Eg – EBtg – Btg - BC
WK6	51° 15′ 50.8″ N 17° 02′ 41.3″ E	176.1	3	Foot slope	Arable land	Haplic Luvisol (Aric, Cutanic, Endoloamic, Ochric, Episiltic, Solimovic)	Ap – AE – Eg – Ab – AEb – EBgb1 – EBgb2 - BCg
WK7	51° 15′ 51.0″ N 17° 02′ 41.0″ E	170.2	2	Toe slope	Arable land	Eutric Solimovic Regosol (Aric, Ochric, Episiltic)	Ap – AE – Eg – 2EBg1 – 2EBg2 – 3C – 4C
WK8	51° 16′ 08.5″ N 17° 02′ 42.0″ E	198.1	7	Shoulder	Arable land	Haplic Luvisol (Aric, Cutanic, Endoloamic, Ochric, Episiltic, Raptic)	Ap – Bt – Bt/BC – 2BCk1 – 2BCk2
WK9	51° 16′ 07.1″ N 17° 02′ 45.8″ E	193.7	12	Shoulder	Arable land	Eutric Regosol (Aric, Endoloamic, Ochric, Episiltic)	Ap – BCk1 – BCk2
WK10	51° 16′ 05.2″ N 17° 02′ 47.5″ E	191.4	7	Back slope	Arable land	Haplic Luvisol (Aric, Cutanic, Endoloamic, Ochric, Episiltic, Raptic)	Ap1/Bt – A2/Bt – Bt -BC1 – BC2
WK11	51° 16′ 03.8″ N 17° 02′ 50.4″ E	188.9	3	Back slope	Arable land	Haplic Luvisol (Aric, Cutanic, Ochric, Siltic)	Ap/Bt – Bt/Ap – BC – BC1 – BC2
WK12	51° 16′ 03.0″ N 17° 02′ 50.0″ E	185.6	2	Foot slope	Arable land	Endostagnic Solimovic Eutric Regosol (Pantosiltic, Ochric)	A/C – A – BC1g – BC2g

ammonium hydroxide and a Beckman–Coulter LS 13 320 laser diffraction analyser at the Leibniz-Institut für Angewandte Geophysik in Hannover, Germany

2.5. OSL dating

Samples for OSL dating were prepared under subdued red-light conditions. The soil material from the outer ~ 2 cm of both sides of the sampling tubes was removed and used for dose-rate determination. Material from the inner part of the tubes was treated with 10% HCl to dissolve the carbonates, 3% sodium oxalate to separate the aggregates and 30% H_2O_2 to remove the organic matter. The fine silt size fraction (4–11 μ m) was separated by sedimentation based on Stoke's law. To obtain a pure quartz fraction for measurement, the sample was treated with 40% H_2SiF_6 acid for 5 days in order to dissolve any remaining feldspars. Fine silt polymineral and quartz extracts were deposited on Al discs (2 mg/disc). All measurements were performed using an automated luminescence reader (Risø TL/OSL-DA-15) equipped with a $^{90}Sr/^{90}Y$ beta source for irradiation. For the polymineral fraction, infrared (870 ± 40 nm) LEDs were used for stimulation, and luminescence signals were detected through a combined filter pack with blue transmission (Schott BG-39 and Corning 7–59). For the quartz fraction blue LEDs (470 ± 30 nm) were applied for stimulation, and the luminescence signals were detected through a 7.5 -mm Hoya U-340 filter with UV transmission. The single-aliquot regenerative (SAR) dose protocols used for dating are shown in Table 2. A low-temperature post-IR IRSL (pIRIR) dating protocol was applied to the polymineral fraction, preheat to 200 °C for 60 s and then with a first IR stimulation at 50 °C (IR_{50}) for 100 s and a second IR stimulation at 170 °C ($pIRIR_{170}$) for 100 s' (Li et al., 2015; Reimann et al., 2011). The first 10 s signal of the decay curve was integrated for equivalent dose (De) estimation with the last 10 s subtracted as background. Six aliquots were measured for each sample. All the aliquots showed good luminescence characteristics, including high signal intensity ($T_n > BG + 3\sigma$), a recycling ratio within 10% of unity, and a recuperation ratio of less than 5%. No aliquot was rejected in D_e estimation. Fading rates (g-values) of the IR_{50} and $pIRIR_{170}$ signals were measured using the SAR protocol (Auclair et al., 2003). Fading correction was performed following the method of Huntley and Lamothe (2001), using the 'calc_FadingCorr' function in the 'Luminescence' R package (Kreutzer et al., 2012). To test the reliability of the SAR protocol for the D_e measurements, samples LUM4248, LUM4253 and LUM4259 were used for dose recovery tests. Five aliquots from each sample were bleached using a Hönle solar simulator (SOL2) for 2 h to remove the natural signal. Two aliquots were used to measure the residual dose and three aliquots were given doses of 50.0, 28.5 and 10.7 Gy for LUM4248, LUM4253 and LUM4259, respectively. Then the aliquots were treated as natural aliquots in order to measure the D_e. The recovered doses (residual dose subtracted) were within 5% of the given doses for both the IR_{50} and $pIRIR_{170}$ signals (Fig. 2).

For the quartz fraction, the preheating treatment involved 220 °C for 10 s, with the OSL signal measured at 125 °C for 40 s. The first 0.5-s signal of the decay curve was used for D_e estimation, with the last 3.2-s signal subtracted as background. For each sample, 10–12 aliquots were measured. Similarly, to the polymineral analysis, the OSL characteristics of the quartz samples were very good and all aliquots passed the rejection criteria. An IR depletion ratio test was performed on each sample and no feldspar contamination was identified (Duller, 2003). A high preheating temperature can induce a thermally transferred OSL signal and result in D_e overestimation, whereas a low preheating temperature may not be able to remove the unstable signals of the regenerative doses, thereby resulting in D_e underestimation (Wintle and Murray, 2006). To test whether the preheating temperature of 220 °C was suitable for the quartz D_e measurements, the D_e values of two samples (LUM4253 and LUM4259) were measured using different preheating temperatures, ranging from 160 to 280 °C, with an interval of 20 °C. This demonstrated that a D_e plateau could be reached using preheating temperatures between 180 and 220 °C (Fig. 3a, b). A dose recovery using different preheating temperatures was performed on LUM4249. A group of aliquots from LUM4249 were bleached in natural sunlight for 30 min in April 2021, in Hannover, Germany. A fixed dose of 14.3 Gy was given to the bleached aliquots. The aliquots were divided into seven groups (with three aliquots in each group) and measured using the SAR protocol and different preheating temperatures. Another group of aliquots were used to measure the residual doses after sunlight bleaching under different preheating temperatures. The residual doses were less than 0.1 Gy for all the aliquots. The recovered doses (residual dose subtracted) were divided by the given dose to obtain the dose recovery ratios. This showed that the recovery ratios were within 2% of unity when the preheating temperature was between 160 and 240 °C (Fig. 3c). Similar dose recovery tests were performed on five more quartz samples, with different given doses from 1.4 to 61 Gy, but with a fixed preheating temperature of 220 °C. All the recovered doses were within 5% of the given doses (Fig. 3d). These results indicate that the measured D_e values were reliable.

The uranium (U), thorium (Th), and potassium (K) concentrations were measured, using gamma spectrometry to calculate the dose rates (Table 3). A 20% radon loss from the ^{238}U series was assumed (Olley

Table 2
Protocols used for dating.

Step	pIRIR protocol for polymineral	Observed	Blue OSL protocol for quartz	Observed
1	Given dose Di		Given dose Di	
2	Preheat at 200 °C for 60 s		Preheat at 220 °C for 10 s	
3	IRSL at 50 °C for 100 s	L_{x1}	OSL at 125 °C for 40 s	L_x
4	IRSL at 170 °C for 100 s	L_{x2}	Test dose	
5	Test dose		Cutheat to 200 °C	
6	Preheat at 200 °C for 60 s		OSL at 125 °C for 40 s	T_x
7	IRSL at 50 °C for 100 s	T_{x1}	OSL bleaching 240 °C for 40 s	
8	IRSL at 170 °C for 100 s	T_{x2}	Return to step 1	
9	IR bleaching at 220 °C for 40 s			
10	Return to step 1			

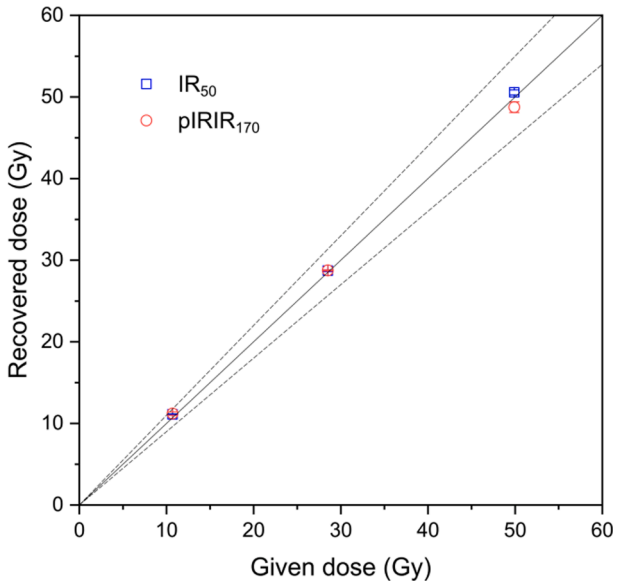

Fig. 2. Dose recovery tests with the $pIRIR_{50,\ 170}$ SAR protocol. Each data point is an average of 3 aliquots. Samples LUM4248, LUM4253, LUM4259 were bleached by the SOL2 for 2 h and given doses of 50.0 Gy, 28.5 Gy, and 10.7 Gy respectively. The recovered doses were within 5% of the given doses.

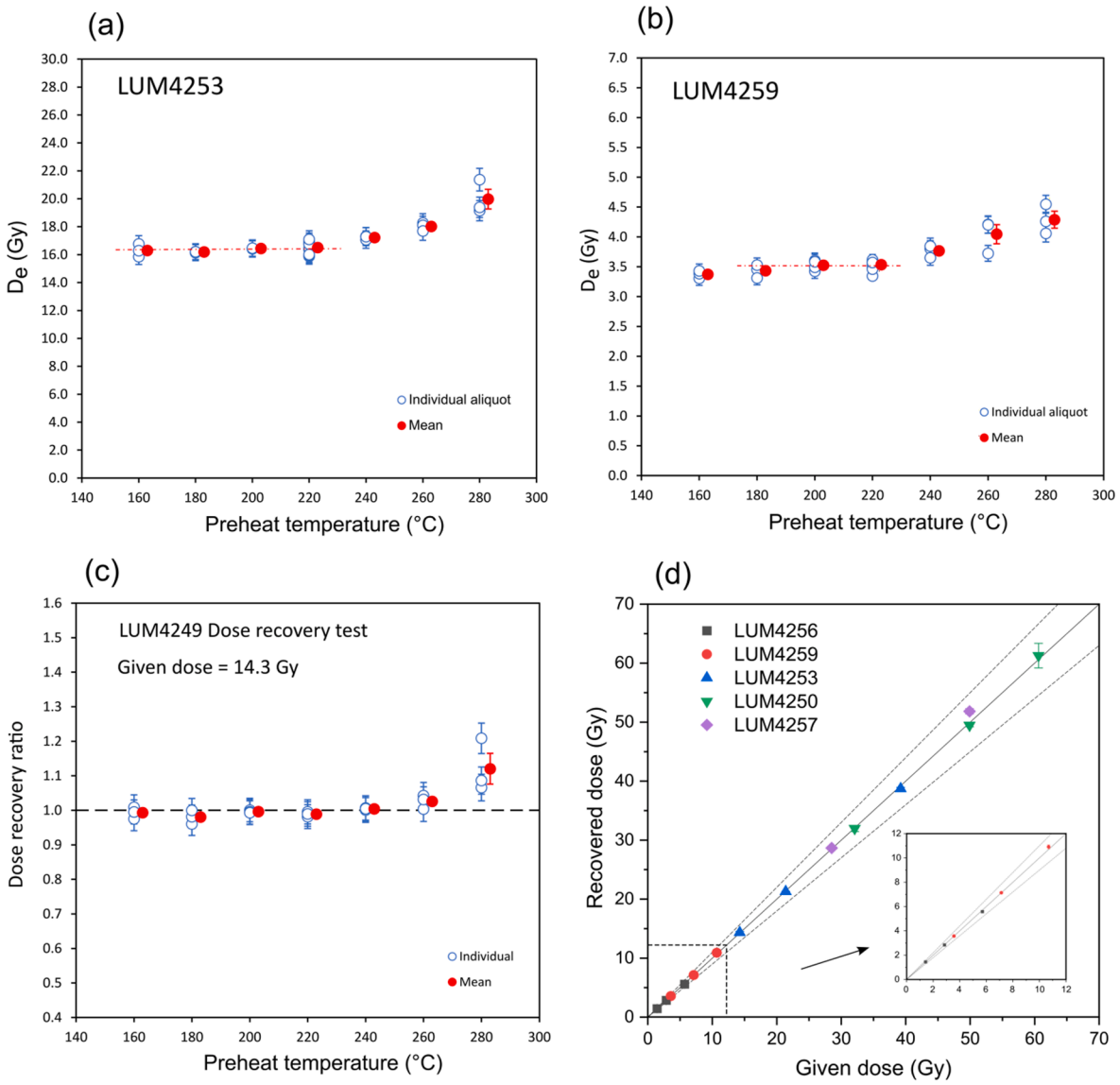

Fig. 3. a) De vs. preheat temperature of LUM4253, b) De vs. preheat temperature of LUM4259, c) Dose recovery ratio vs. preheat temperature of LUM4249, d) Recovered doses vs. given doses with a fixed preheat temperature at 220 °C.

et al., 1997). Conversion factors from Liritzis et al. (Liritzis et al., 2013) were applied. The *a*-value was taken as 0.04 ± 0.02 (Rees-Jones and Tite, 1997). The cosmic dose rate was estimated based on the sample depth, altitude, and geographical coordinates of each sample (Prescott and Hutton, 1994). Water content of 20 ± 5% was used for all samples.

2.6. *Verification of the reliability of OSL ages*

The dose rates are summarised in Table 4. It is well known that the quartz OSL signal is much easier to be bleached than the feldspar IRSL signal (Godfrey-Smith et al., 1988; Thomsen et al., 2008; Wallinga, 2002), and that the pIRIR signal is even harder to be bleached than the IR_{50} signal (Buylaert et al., 2011; Chen et al., 2013). Because the fading-corrected $pIRIR_{170}$ ages are always greater than the fading-corrected IR_{50} ages (Table 4), we assumed that the $pIRIR_{170}$ signal of the samples was not fully bleached before deposition and that the corresponding ages were overestimated. For most of the samples, the fading-corrected IR_{50} ages were consistent with the quartz OSL ages (age ratios within 10% of unity, considering the error), indicating that both the IR_{50} and OSL signals were fully reset before deposition. However, for several samples, the fading-corrected IR_{50} ages were still greater than the quartz OSL ages, with an overestimation of up to 140% (e.g. LUM4255, LUM4262), indicating incomplete resetting of the IR_{50} signal before deposition. Thus, to check whether the OSL signal for these samples was fully reset, we applied the method proposed by Murray et al. (2012), by comparing the D_e values between the IR_{50} and quartz OSL signals. For a sample with an OSL signal that had been fully reset before deposition, the difference between the measured and predicted D_e values of IR_{50} should have been less than the acceptance limit, termed as ΔF in Murray et al. (2012). The ΔF is dependent on the size of the measured De of the quartz OSL, and it can be determined based on the different bleaching rates of quartz OSL and feldspar IR_{50} signals (Murray et al., 2012). In Fig. 4, example data for ΔF at several different quartz D_e values are given, taken from Murray et al. (2012), and the dashed line was fitted using these example data. It should be noted that the expected D_e values of IR_{50} were calculated by multiplying the dose rates of the polymineral fine-grained material with the quartz OSL ages and a fading factor. Murray et al. (2012) applied a fading factor of 0.55, based on the study of Buylaert et al. (2012) which showed that the fading uncorrected IR_{50} ages made up about 0.55 of the independent ages. In our study, the ratios of fading-uncorrected IR_{50} ages to fading-corrected IR_{50} ages were between 0.80 and 0.91 for all samples, with a mean ratio of 0.84. Thus, we

Table 3
Dose rates of quartz and polymineral fine grains.

Sample ID	Profile	Horizon	Depth (m)	U (ppm)			Th (ppm)			K (%)			Water (%)			Dose rate (Gy/ka)					
																Quartz			Polymineral		
LUM4245	WK2	BC1	0.52	2.55	±	0.13	8.32	±	0.42	1.79	±	0.09	20	±	5	3.00	±	0.13	3.44	±	0.17
LUM4247	WK3	Bt1	0.45	2.50	±	0.13	9.05	±	0.46	1.88	±	0.10	20	±	5	3.12	±	0.14	3.58	±	0.18
LUM4249	WK4	E	0.54	2.44	±	0.13	7.20	±	0.37	1.71	±	0.09	20	±	5	2.81	±	0.12	3.25	±	0.16
LUM4250	WK5	Eg	0.58	2.21	±	0.11	7.81	±	0.40	1.79	±	0.09	20	±	5	2.87	±	0.13	3.22	±	0.16
LUM4251	WK5	BC	1.17	2.11	±	0.11	8.14	±	0.41	1.63	±	0.08	20	±	5	2.72	±	0.12	3.28	±	0.16
LUM4252	WK6	Eg	0.36	1.95	±	0.10	7.11	±	0.36	1.61	±	0.08	20	±	5	2.62	±	0.11	3.12	±	0.16
LUM4253	WK6	EBgb1	1.02	2.07	±	0.11	6.60	±	0.34	1.60	±	0.08	20	±	5	2.56	±	0.11	2.99	±	0.15
LUM4255	WK7	2EBg2	0.90	1.56	±	0.11	5.64	±	0.33	1.37	±	0.07	20	±	5	2.17	±	0.09	2.74	±	0.14
LUM4257	WK8	Bt/BC	0.52	2.08	±	0.11	7.82	±	0.40	1.73	±	0.09	20	±	5	2.79	±	0.12	2.93	±	0.15
LUM4259	WK10	BC2	1.04	2.20	±	0.11	7.73	±	0.39	1.70	±	0.09	20	±	5	2.77	±	0.12	3.19	±	0.16
LUM4260	WK11	BC2	1.05	1.69	±	0.09	6.31	±	0.33	1.39	±	0.07	20	±	5	2.27	±	0.10	3.17	±	0.16
LUM4261	WK12	BC1g	0.62	2.31	±	0.12	8.09	±	0.41	1.67	±	0.09	20	±	5	2.81	±	0.12	2.60	±	0.13
LUM4262	WK12	BC2g	1.24	2.47	±	0.13	8.19	±	0.42	1.72	±	0.09	20	±	5	2.88	±	0.13	3.23	±	0.16

applied a fading factor of 0.84 to calculate the predicted D_e of IR_{50}. Consequently, we also adjusted the ΔF data from Murray et al. (2012), multiplying it by a factor of 1.53 (i.e. 0.84/0.55). It can be seen from Fig. 4 that all samples, except for two from profile WK7 (LUM4254, LUM4256), plotted below the acceptance limit, indicating that the quartz OSL of these samples was fully reset before deposition and that the quartz OSL ages were reliable. For sample LUM4260, the measured IR_{50} D_e was even smaller than the predicted IR_{50} D_e. The reason for this might be that the measured fading rate for LUM4260 was underestimated. It should also be noted that, even when applying a fading factor of 0.55, as used in Murray et al. (2012), all the samples still plotted below the acceptance limit line. It was reasonable for Murray et al. (2012) to use a higher fading factor than in this study because, in their study, the IR_{50} signal was measured after a preheating treatment of 320 °C. It has been widely reported that when a high preheating temperature (e.g. > 250 °C) is used, the dose recovery ratio of the IR_{50} using the SAR protocol is always underestimated due to failure of the sensitivity correction in the first cycle (Kars et al., 2014; Qin et al., 2018; Wallinga et al., 2000; Zhang, 2018). The IR_{50} D_e underestimation resulting from the failure of the sensitivity correction was also incorporated into the fading factor in Murray et al. (2012). In our study, the preheating temperature was set at just 200 °C. The D_e was not further underestimated by failure of a sensitivity correction, and the fading factor was thus larger.

2.7. Radiocarbon dating.

Three samples of secondary carbonate nodules were measured by accelerator mass spectrometry using 1.5 SDH Compact Pelletron (National Electrostatics Corporation, Middleton, USA) at the Poznan Radiocarbon Laboratory. Calendar ages were obtained using the OxCal 4.4 calibration program (Bronk Ramsey, 2009, 2001) based on the IntCal 13 calibration curve (Reimer et al., 2013). The calibrated ages are given in the 2σ range (minimum and maximum value for each) (Table 5).

3. Results

3.1. Visualisation of lithology using the ERT tool

The ERT measurements allowed visualisation of the variability of the geological structure of the shallow ground and distinction of the main lithological units (Fig. 1). All investigated rock formations had relatively low electrical resistivity (Fig. 1). It was difficult to relate them directly to existing geological data because there were no boreholes through the Quaternary sediments in the vicinity of the surveyed sections. There are boreholes ~ 4 km to the south-east through the footslope of the studied hills (Pierwoszów 1) and 6 km to the north (Trzebnica IG-1), but both penetrate a different, higher morphological position (Winnicki, 1997, 1990, 1985).

Nevertheless, based on interpretations from those boreholes, it was assumed that the AB inversion model also represented pre-Quaternary sediments. These might be glacigenically deformed Miocene clays (Section a in Fig. 1) overlain by two or three generations of Quaternary sediments (Subdivisions b and c), which were interpreted as sequences of glacial deposits. Two thin layers of slope sediments (d) were visible in the ground surface zone, including thicker colluvium at the base of the slope (e).

3.2. Soil classification and morphology

The field soil survey, including the profiles (Fig. 5) and drillings, confirmed loess thicknesses that varied between 1 and 1.2 m in stable landscape positions (top slope with 4° inclination), where relatively complete Luvisols with preserved E and Bt horizons had developed (WK1). The rest of the studied soils revealed morphologies shaped by

Table 4
The De values and OSL ages.

Sample ID	Profile	Horizon	Signal	D_e (Gy)			Apparent age (ka)			g_{2d} (%/decade)			Fading corrected age (ka)			Age ratio IR_{50}/quartz		
LUM 4245	WK2	BC1	OSL	49.6	±	1.1	16.6	±	0.8							1.01	±	0.08
			IR_{50}	46.5	±	0.4	13.5	±	0.7	3.24	±	0.00	16.8	±	0.9			
			$pIRIR_{170}$	66.0	±	0.4	19.2	±	1.0	1.27	±	0.27	20.8	±	1.1			
LUM 4247	WK3	Bt1	OSL	45.2	±	1.1	14.5	±	0.7							0.92	±	0.07
			IR_{50}	39.4	±	0.2	11.0	±	0.6	2.96	±	0.06	13.3	±	0.7			
			$pIRIR_{170}$	52.3	±	0.2	14.6	±	0.7	1.14	±	0.06	15.7	±	0.8			
LUM 4249	WK4	E	OSL	10.7	±	0.1	3.8	±	0.2							1.16	±	0.08
			IR_{50}	12.0	±	0.1	3.7	±	0.2	2.87	±	0.04	4.4	±	0.2			
			$pIRIR_{170}$	16.9	±	0.4	5.2	±	0.3	1.11	±	0.08	5.6	±	0.3			
LUM 4250	WK5	Eg	OSL	26.2	±	0.2	9.1	±	0.4							1.39	±	0.10
			IR_{50}	34.1	±	0.3	10.4	±	0.5	3.06	±	0.03	12.7	±	0.7			
			$pIRIR_{170}$	44.6	±	0.5	13.6	±	0.7	1.15	±	0.05	14.6	±	0.8			
LUM 4251	WK5	BC	OSL	40.9	±	0.8	15.1	±	0.7							1.00	±	0.07
			IR_{50}	38.2	±	0.2	12.2	±	0.6	3.17	±	0.09	15.1	±	0.8			
			$pIRIR_{170}$	51.7	±	0.3	16.5	±	0.8	1.27	±	0.14	17.9	±	0.9			
LUM 4252	WK6	Eg	OSL	1.8	±	0.0	0.7	±	0.03							1.17	±	0.08
			IR_{50}	2.2	±	0.1	0.73	±	0.04	2.28	±	0.07	0.82	±	0.05			
			$pIRIR_{170}$	3.9	±	0.1	1.30	±	0.08	0.61	±	0.25	1.34	±	0.08			
LUM 4253	WK6	EBgb1	OSL	16.5	±	0.1	6.4	±	0.3							1.33	±	0.09
			IR_{50}	20.8	±	0.2	7.1	±	0.4	2.94	±	0.07	8.6	±	0.5			
			$pIRIR_{170}$	28.3	±	0.3	9.7	±	0.5	1.53	±	0.09	10.6	±	0.6			
LUM4255	WK7	2EBg2	OSL	3.3	±	0.1	1.5	±	0.1							2.43	±	0.17
			IR_{50}	7.5	±	0.1	3.0	±	0.2	3.31	±	0.19	3.68	±	0.2			
			$pIRIR_{170}$	20.2	±	0.9	8.2	±	0.5	1.11	±	0.19	8.72	±	0.6			
LUM 4257	WK8	Bt/BC	OSL	48.0	±	1.8	17.2	±	1.0							0.93	±	0.07
			IR_{50}	41.1	±	0.2	12.9	±	0.6	3.25	±	0.12	16.0	±	0.8			
			$pIRIR_{170}$	62.1	±	0.9	19.5	±	1.0	0.68	±	0.21	20.3	±	1.1			
LUM 4259	WK10	BC2	OSL	3.5	±	0.0	1.3	±	0.1							1.75	±	0.12
			IR_{50}	6.1	±	0.1	1.9	±	0.1	2.67	±	0.08	2.2	±	0.1			
			$pIRIR_{170}$	11.4	±	0.2	3.6	±	0.2	0.78	±	0.11	3.7	±	0.2			
LUM 4260	WK11	BC2	OSL	60.3	±	3.1	26.6	±	1.8							0.78	±	0.07
			IR_{50}	43.7	±	0.2	16.8	±	0.8	3.07	±	0.13	20.7	±	1.1			
			$pIRIR_{170}$	88.0	±	0.4	33.9	±	1.7	1.28	±	0.23	36.9	±	2.0			
LUM 4261	WK12	BC1g	OSL	1.2	±	0.0	0.4	±	0.02							1.35	±	0.10
			IR_{50}	1.7	±	0.0	0.5	±	0.03	2.08	±	0.04	0.57	±	0.03			
			$pIRIR_{170}$	4.7	±	0.1	1.5	±	0.08	0.09	±	0.16	1.47	±	0.09			
LUM 4262	WK12	BC2g	OSL	4.4	±	0.0	1.5	±	0.1							1.88	±	0.13
			IR_{50}	8.2	±	0.1	2.5	±	0.1	2.79	±	0.17	2.9	±	0.2			
			$pIRIR_{170}$	17.7	±	0.2	5.3	±	0.3	1.04	±	0.14	5.7	±	0.3			

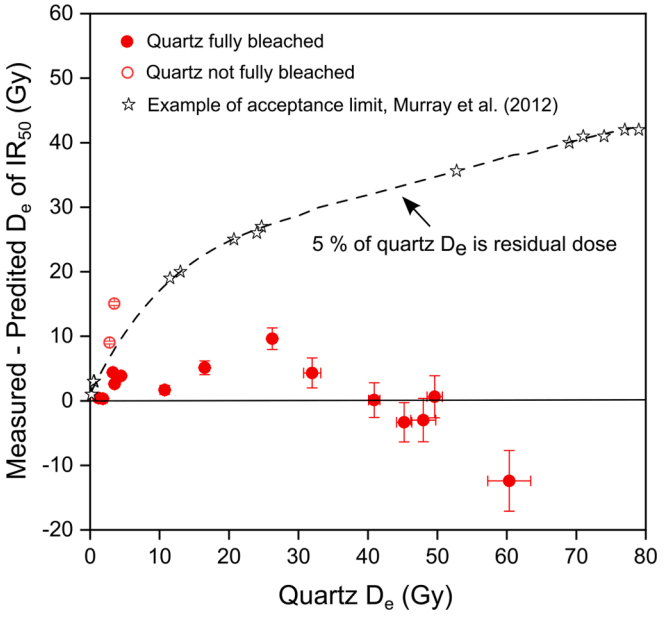

Fig. 4. The differences between measured and predicted D_e values of IR_{50} plotted against the measured quartz D_e. The dashed line indicates the acceptance limit. If a sample is plotted under the dashed line, it indicates that the quartz OSL signal of this sample has been fully bleached before deposition.

Table 5
Radiocarbon ages of carbonate hard nodules.

Soil profile/ soil horizon	Depth (cm)	Lab code	Uncalibrated ^{14}C age (yr BP)	Calibrated age (2-sigma range (95.4%)) cal BC
WK7/4Cgk	120	Poz-112868	6860 ± 50	5843–5640
WK8/ 2Bck2	82	Poz-120446	1700 ± 60	11718–11501
WK9/BCk1	35	Poz-120447	16020 ± 80	17587–17181

denudation processes. Erosion processes led to a thinning of the loess mantle that had substantial morphological consequences, resulting in the removal of the E horizon and further incorporation of the Bt horizon into the Ap horizon due to ploughing (WK2, WK3, WK8, WK10, WK11). In extreme cases, the Bt horizon was not a master horizon but a part of a transitional horizon (Table 1) with a thickness of only 14 cm. Progressive erosion, causing a shallowing loess mantle, may have also resulted in the exhumation of underlying coarse-grained materials (e.g., in WK9). The deposition of eroded material from the upslope was recorded in the mid-and foot-slope positions of both transects. In the south-trending transect, its presence was observed in profiles WK4 and WK5, expressed as much thicker topsoil (A, AE and E, EB horizons), while in WK6, we detected a buried A horizon covered with 45 cm of slopewash sediment. Profile WK7 represented the stratification of fine- and coarse-grained (with diagonal lineation) colluvium over glacial till. In the eastern transect, clear morphological features of accumulation were

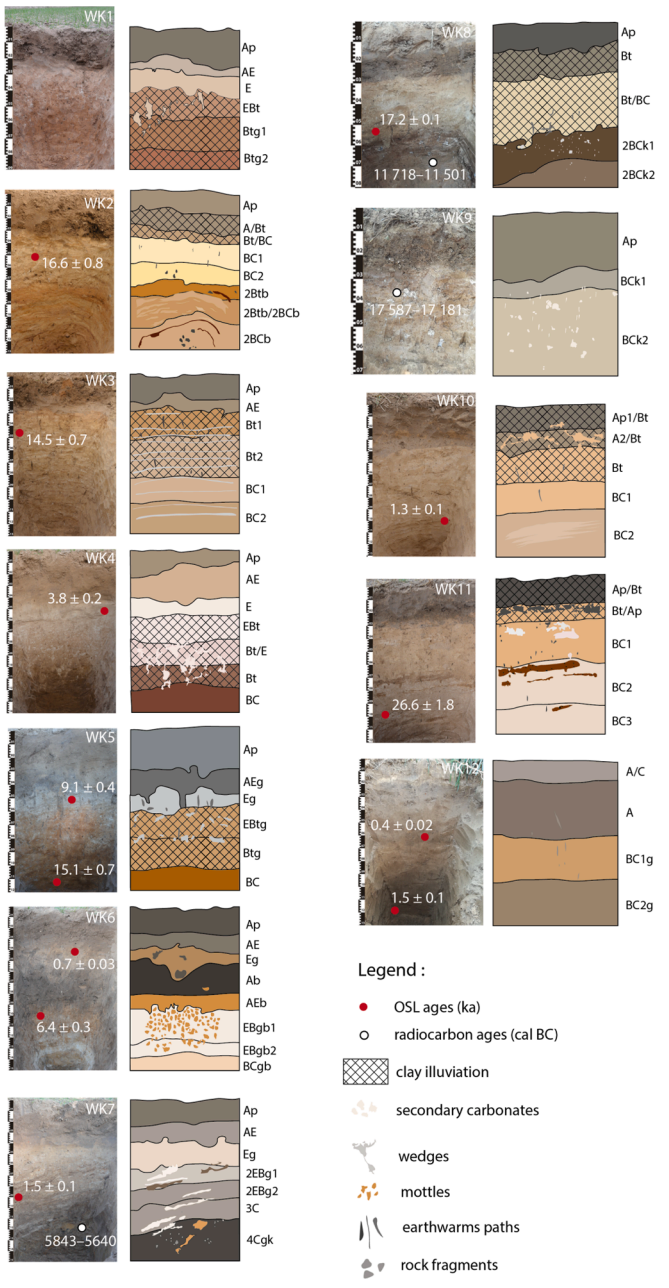

Fig. 5. Photos and sketches presenting morphology of studied soil profiles and sampling positions for OSL dating with obtained ages.

detected only in WK12, which had 60 cm of colluvium. Loess mantles are carbonate free; however, hard carbonate nodules and coatings were found in the glacial materials of the WK7, WK8 and WK9 sites.

Although most of the soils had experienced erosion processes, almost all were classified as Luvisols (Table 1). Because the topsoil horizons did not meet the criteria for being mollic or chernic (too high values and chromas), they still (in the case of strongly eroded pedons, e.g., WK2/WK3) had argic horizons. Profiles WK7, WK9 and WK12 fell into the Regosol reference group because no diagnostic horizons were recognised in these. Detailed information on the physicochemical properties is available in Loba et al. (2021)

3.3. Grain size distribution

In the profiles, the most dominant fraction was coarse silt (45–50 μ m) (Fig. S1), which is typical of loess deposits. However, the grain size distribution also indicated certain differences. Materials deposited during MIS 2 have a narrow peak range between 44 and 48 μ m, whereas younger sediments are bimodal (Fig. 6A), with dominant coarse silt (35–58 μ m) and medium sand (210–550 μ m) fractions. In the soils characterised by lithic discontinuities, the most pronounced fractions in the lower horizons tended to be in the medium sand range (102–104 μ m), as in WK2, or were multimodal, with their highest peaks at 8, 50 and 120 μ m (WK8) or 7, 49 and 230 μ m (WK9). In WK6 and WK10, the fractions were bimodal, the highest peak being within the range of coarse silt (45–49 μ m) and the smaller peaks within the range of medium sand (370 μ m) (Fig. 6B).

3.4. Soil micromorphology

The thin sections revealed mostly a subangular and crumby type of microstructure (e.g. WK6, WK12), with vugs and plane types of voids. Sometimes, a void chamber type was recognised (e.g. in WK2, WK3, WK6). The groundmass was characterised by enaulic and porphyric coarse:fine (c:f) related distribution patterns, albeit with various coarse and fine size limits (Table S1). The b-fabric of the horizons varied from porostriated, to granostriated and randomly striated, with rare monostriated to speckled or stipple-speckled patterns. The soils from the toe slope mostly had undifferentiated b-fabric patterns (Table S1).

The most common pedofeatures were typic and, rarely, concentric or aggregate Fe-hydroxide nodules with weak and moderately

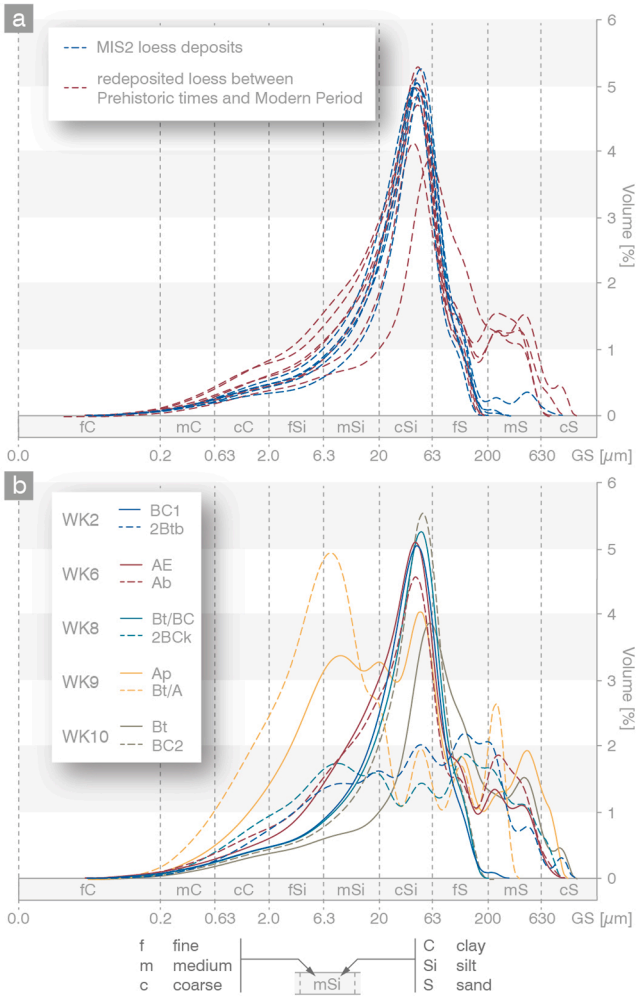

Fig. 6. Grain-size curves illustrating main modes in a) loess sediments deposited during MIS2 and redeposited between Prehistoric times to Modern Period, and b) soils with the textural contrast.

impregnation, and having orthic and/or anorthic character (e.g., Fig. 7A: c, e, h and Fig. 7B: c, d).

The expression of clay pedofeatures differed in the soils along the transects. The best-developed illuviation features were recognised in WK2 (Bt/BC), which exhibited mostly fragmented, dense, incomplete and loose, continuous dusty clay infillings (Table S1), but also fine yellowish-brown clay coatings were found in that profile (Fig. 7A: a). Horizon 2Bt/2BCg of WK2 revealed more definite features related to clay illuviation; however, the typical coatings or infillings were not always formed, with the clay occurring mostly around grains and as yellowish-brown, elongated, limpid aggregations of fine clays (with no laminations), often broken and heterogeneously distributed in the groundmass (Fig. 7A: b).

The soil profiles from the middle section of the slopes (WK3, WK4, WK8, WK9) showed weak clay illuviation characteristics, but their abundance and typology differed. The Ap horizon of WK3 had a very high content of microlaminated coatings of limpid yellowish-brown clay, often disrupted and fragmented (Fig. 7A: c, d). However, some well-developed laminated yellowish-brown clay coatings also occurred (Fig. 7A: d). Moreover, a lot of fine, dense, incomplete fragmented clay infillings were found (Fig. 7A: c). The lower horizons (Bt1, Bt2, Bt/E) similarly showed microlaminated, but very small and strongly fragmented, yellowish-brown clay coatings and single, weakly and moderately developed laminated clay coatings (Fig. 7A: e–g), as well as fragmented and small, dense, incomplete and loose continuous clay infillings. The illuvial clay features indicated disturbance of the illuviation process, mainly due to mass wasting. We observed many illuvial features in the Ap horizon, as the Bt horizon was partially incorporated into that. Apart from occasional occurrences of non-laminated, very fragmented yellowish-brown coatings of illuvial clay in the Bt horizon of WK8 (Fig. 7B: a), there were no other signs of clay illuviation in the soils. Furthermore, a large quantity of geodic calcite nodules, along with calcitic coatings/hypocoatings, were found in the Bt/BC horizon of WK8 (Fig. 7B: b). Profiles from the backslope and toe slopee (WK6, WK11, WK12), apart from very residual and fragmentary clay coatings (Fig. 7B: c, d), generally exhibited no pedofeatures typical of clay illuviation. Only the Eg and EBgb1 horizons of WK6 and BC1g of WK12 contained fragments of disrupted, microlaminated, illuvial reddish-brown clay coatings (Fig. 7A: h and 7B: e, f, respectively). Their morphology and size suggested an ex-situ origin, probably an effect of the slopewash.

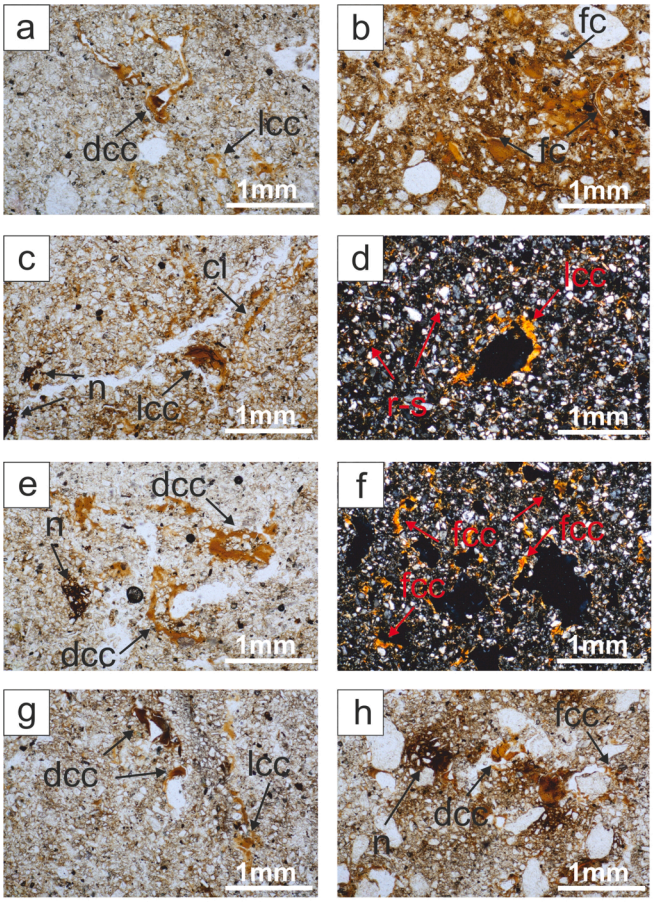

Fig. 7A. Microphotographs of soil thin sections showing alternating clay illuvial pedofeatures relative to location on the slopes. (a) profile WK2, horizon Bt/BC: dcc – dusty layered clay illuvial coatings, lcc – limpid layered clay illuvial coatings, PPL; (b) profile WK2, horizon 2Bt/2BCg: fc – yellowish-brown elongated fine clay aggregations, PPL; (c) profile WK3, horizon Ap: dcc – displaced and fragmented microlaminated limpid clay illuvial coatings, ci – dense incomplete, loose discontinuous clay infillings, n – weakly impregnated anorthic Fe hydroxide nodules, PPL; (d) profile WK3, horizon Ap: llc – fragmented layered limpid clay illuvial coatings, r-s – random-striated b-fabric pattern, XPL; (e) profile WK3, horizon Bt1: dcc – fragmented layered dusty clay illuvial coatings, n –moderately impregnated anorthic Fe hydroxide nodules, PPL; (f) profile WK3, horizon Bt1: fcc – fragmented microlaminated clay illuvial coatings, XPL; (g) profile WK4, horizon Bt/E: dcc – fragmented microlaminated dusty clay illuvial coatings, lcc – microlaminated limpid clay illuvial coatings, PPL; (h) profile WK6, horizon EBgb1: dcc – dusty microlaminated clay illuvial coatings, fcc – fragmented microlaminated clay illuvial coatings, n – moderately impregnated anorthic Fe hydroxide nodules, PPL. Bar length = 1 mm.

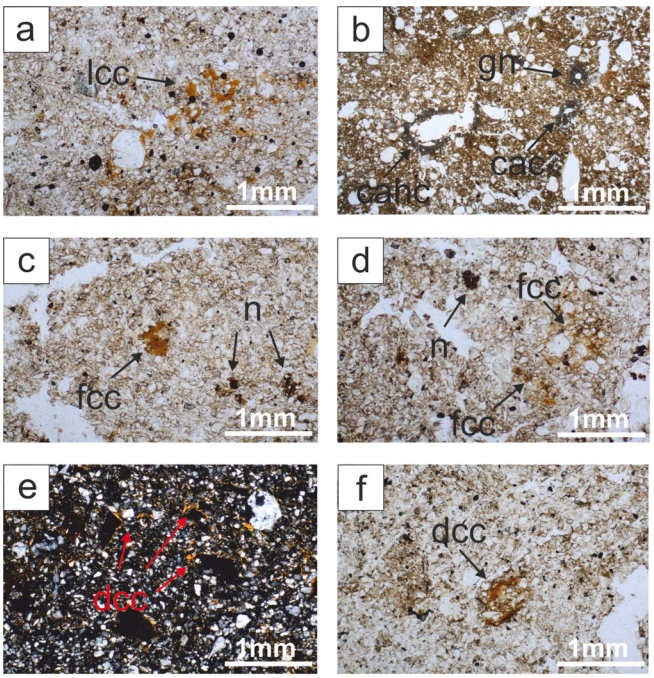

Fig. 7B. Microphotographs of soil thin sections showing alternating clay illuvial pedofeatures relative to location on the slopes. (a) profile WK8, horizon Bt: lcc – fragmented microlaminated limpid clay illuvial coatings, PPL; (b) profile WK8, horizon Bt/BC: gn – geodic calcitic nodules, cac – calcitic coatings, cahc – calcitic hypocoatings, PPL; (c) profile WK11, horizon Ap/Bt–Bt/Ap: fcc – displaced and fragmented microlaminated clay illuvial coatings, n – weakly impregnated anorthic Fe hydroxide nodules, PPL; (d) profile WK11, horizon Bt/Ap: fcc – strongly fragmented and microlaminated clay illuvial coatings, n – moderately impregnated anorthic Fe hydroxide nodules, PPL; (e) profile WK12, horizon BC1g: dcc – fragmented dusty clay illuvial coatings, XPL; (f) profile WK12, horizon BC1g: dcc – fragmented and microlaminated dusty clay illuvial coatings, PPL. Bar length = 1 mm.

3.5. OSL and ^{14}C dating

The luminescence ages from the soil profiles represent a wide

timespan. Most of the ages correlated to MIS 2 (LUM 4245, LUM 4247, LUM 4251, LUM 4257, LUM 4260), but also to the Prehistoric times (9.1 ± 0.4 ka; LUM4250), the Neolithic (6.4 ± 0.3 ka; LUM 4253) and the Bronze Age (1.5 ± 0.1 ka; LUM 4249). The youngest dates relate to the Middle Ages and the early Modern, with a minimum age of ~ 0.4 ka (Table 4). Moreover, two samples (LUM4258, LUM4246) from the bottom parts of WK2 and WK9, respectively, were saturated with luminescence signals from both quartz and feldspar because they were much older than the last glaciation. Radiocarbon ages for the hard carbonate nodules covered a broad spectrum, from 17.5 to 5.4 cal ka BP (Table 5).

4. Discussion

4.1. Record of denudation events

The OSL dating suggested that the loess deposits in their lowermost horizons (BC and C) were LGM or late glacial in age (Table 4), which is typical for the thin aeolian-silt mantle in the southwestern Poland (Moska et al., 2019; Waroszewski et al., 2021). In the toe slopes, however, the ages for the uppermost eluvial horizons indicated sediment redeposition along the slope due to erosional processes and their termination as colluvial deposits (Table 4). Based on our OSL ages, we assumed that the first phase of redeposition occurred ~ 9.1 ka (profile WK5), at the transition from the Preboreal to the Boreal. This could be related to cold and dry climatic oscillations that triggered natural forest fires and, as a consequence, soil erosion and colluviation (Dreibrodt et al., 2010a, 2010b; Kołodyńska-Gawrysiak et al., 2018). It seems that, following this event, slope-washing processes were intensified no earlier than the Neolithic. A record of this colluviation was detected in WK6 (6.4 ± 0.3 ka). The acceleration of soil erosion was probably related to the Linear Pottery culture that settled the area of the Central European loess belt at that time, after which vast forested areas were gradually transformed into farmland (Dreibrodt and Bork, 2021; Gerlach et al., 2012; Poręba et al., 2011; Starkel et al., 2013). Also, the burning (slash and burn) practices to prepare arable lands and obtain high crop yields that were typical during the Neolithic may have increased soil erosion rates (Gerlach et al., 2012). However, we did not find pyrogenic features in the studied soils. Later, another phase of redeposition occurred that was recorded in WK4 (LUM 4249). This particular phase was attributed to the transition from the Early to Middle Bronze Age (3.8 ± 0.2 ka), when the climate was cold and humid (Dotterweich, 2008) and there was an expansion of the human population and farming activities (Kołodyńska-Gawrysiak et al., 2017; Rejman and Rodzik, 2006). However, colluvial sediments corresponding to this period have been found in Germany and other parts of Poland (Döhler et al., 2015; Kołodyńska-Gawrysiak et al., 2018, 2017; Poręba et al., 2011), whereas, in southwest Poland, there is a lack of such data. The ages from WK6, WK7 and WK10 correspond to the early (1.5 ± 0.1 ka to1.3 ± 0.1 ka) and late (0.7 ± 0.03 ka) Middle Ages. At the beginning of the Middle Ages, the climate was warm and temporarily dry, however, in the later period, the summers were wet and rainy, leading to flooding (Dotterweich, 2008; Dreibrodt and Bork, 2021). The signal for the last episode of soil erosion (WK12) came from the early Modern (0.4 ± 0.02 ka) and corresponded to the Little Ice Age, when the temperature decreased and precipitation rates increased, and mass processes on slopes were consequently accelerated (Starkel, 2005).

The progressive denudation led to the exhumation of deposits older than the loess that is not suitable for dating due to their saturated luminescence signals. These deposits include the lowermost horizons of WK2 (LUM4246) and WK9 (LUM4258). Denudation intensity is also expressed in grain size composition. Soil has a limited infiltration capacity, so, during intensive rainfall, surface runoff occurs and sediment is transported in the flow (Morgan, 2005; Wacha et al., 2018). The redeposited sediments (Fig. 6A) had dominant coarse silt fractions but also exhibited peaks in medium sand. The climate during this time was humid/wet (Starkel, 2005), and thus favourable to erosion processes because the highest detachment of soil particles is at the beginning of a storm and the transport capacity is reached very quickly (Morgan, 2005). Such conditions enabled the transport of medium-sand-sized particles that could have originated from coarser loess deposits or older substrates, such as glaciofluvial materials, that occurred in the upper/middle slope positions.

The broad time over which the sediments were redeposited is in agreement with the findings from other studies on Central Europe. For instance, Dotterweich et al. (2012), Kołodyńska-Gawrysiak et al. (2018), Dreibrodt et al. (2013) and Scherer et al. (2021) reported colluvial deposits from eastern Poland and Germany as corresponding to the Neolithic and Bronze Age, respectively. The erosion/deposition processes were intensified in the Middle Ages due to the development of new tools for agriculture, which enabled the expansion of arable land, as presented by Dreibrodt and Bork (2021), Dreibrodt et al. (2013), Poręba et al. (2011), Döhler et al. (2015), Dotterweich (2008) and Dotterweich et al. (2013, 2012). In the late Middle Ages, climatic anomalies, such as long, cold winters and wet rainy summers, probably also affected the intensity of soil erosion (Dreibrodt and Bork, 2021; Starkel, 2005). Furthermore, the increase in land-use intensity continued into the beginning of the Modern Times (Dreibrodt and Bork, 2021), then becoming amplified in the 20th century due to agricultural mechanization (Kopittke et al., 2019).

The denudation processes, however, were nonlinear on the convex (first transect) and concave (second transit) slopes of the study site. The age of the colluvium materials varied considerably in a catenary arrangement. For example, the colluvium making up the topsoil in WK4 and WK5 had a wide age range of deposition—3.8 ± 0.2 ka and 9.1 ± 0.4 ka, respectively. In the second transect, young colluvium (1.3 ± 0.1 ka) in WK10 was followed by a much older bed (~26.6 ± 1.8 ka) in nearby WK11. This diversity in the OSL ages supports a dynamic denudation system and reveals the presence of multiple erosion/accumulation events that occurred in the Holocene. This illustrates their utility in the reconstruction of environmental change because they enable the tracing of denudation events and can identify which layer/horizon was redeposited/truncated.

4.2. Disappearance of Luvisols

In loess areas, soils with or without erosion features create a mosaic pattern along sloping regions that are shaped by denudation processes. The loess was deposited as thick sediments around the LGM in Lower Silesia and, according to the radiocarbon ages of hard carbonate nodules, they were decalcified during two older phases ~ 17 and 11 ka, while the youngest decalcification took place around 5 ka (Table 5). At the end of the Pleistocene/early Holocene, Chernozems (Altermann et al., 2005; Eckmeier et al., 2007; Kabała et al., 2019; Kołodyńska-Gawrysiak et al., 2017; Labaz et al., 2018) most likely developed in the loess. We can hypothesise that they were preserved until the Neolithic (Kabała et al., 2019), at which point they began to degrade into Luvic Chernozems/Pheozems and finally into Luvisols (Drewnik and Żyła, 2019; Zádorová et al., 2014). This last step in their transformation was evidenced in our study site, with Luvisols being the dominant soil group, revealing varied morphologies as a result of multiple erosion/accumulation events, dependant on the dynamics of slope processes. In the middle slope and toe slope sections (WK4, WK6, WK7), colluvial materials (Neolithic/Bronze Age/Medieval) served as a substrate for the development of thick eluvial horizons. In the slope zones where soil erosion reached its peak, a progressive shallowing of the loess mantle was observed, and consequently, a significant modification of the soil morphology took place. Thus, truncated Luvisols developed as a direct effect of eluvial horizon mixing due to ploughing into the Ap horizon (WK3). However, more extreme cases existed, where argic horizons (Bt) were incorporated into surface humus horizons (WK2, WK10, WK11). In such situations, the A horizons contained clay coatings (Fig. 7) originating from the aggregates of the Bt horizon being dragged up during

agricultural activities. With time, there was a progressive shallowing of the Bt horizons, leading to their complete disappearance. Further thinning of the loess mantle resulted in the exhumation of older sediments, such as glacial tills and glaciofluvial substrates, with no, or very weak, pedogenic alternations (WK9), which led to transformation of the soil into Regosols (Fig. 8). Eroded material was transported downslope and was usually deposited in toeslope positions, forming colluvial soils. The relatively deep colluvium (WK12), being a fresh substrate, may have contained some clay coatings inherited from the eroded Bt horizons (Fig. 7B), but did not have any diagnostic horizons, meaning that it also fell into the Regosol soil reference group. In the young morainic landscape of northern Poland, this kind of direct exposure of the Bt horizon at the soil surface resulted in the formation of Calcisols or Regosols (Radziuk and Świtoniak, 2021; Świtoniak et al., 2016) and led to severe modifications of organic matter and nutrient pools. In Central Europe a transformation of Luvisols due to shallowing of Bt horizons as a consequence of intense soil erosion processes and formation of colluvial soils in the lower parts of slopes is also observed in catenary research of loess areas of Czechia (Strouhalová et al., 2020; Zádorová et al., 2014, 2013; Zádorová and Penížek, 2018), southwestern Germany (Leopold et al., 2011; Scherer et al., 2021; Terhorst, 2000), eastern Poland (Klimowicz and Uziak, 2001; Paluszek, 2013; Rejman et al., 2014b, 2014a; Rejman and Iglik, 2010), southern Poland (Dudek et al., 2022; Glina et al., 2014; Labaz et al., 2022, 2018; Poręba et al., 2015), Belgium (Nachtergaele and Poesen, 2002; Rommens et al., 2005), France (Jagercikova et al., 2015, 2014; Krekelbergh et al., 2020) and in young morainic landscape of western Lithuania (Jarašiūnas et al., 2020).

Recent research on short-term erosion rates conducted on soils developed from loess deposits, by Loba et al. (2021), clearly showed that modern soil erosion rates have considerably increased and considerably exceed soil production rate, and therefore soil transformation will move towards the disappearance of productive Luvisols in arable landscapes. The soil degradation resulting from erosion events causes a shallowing of the loess solum, depletion in organic matter and nutrients and a reduction in crop productivity, mostly due to a decrease in the retention capacity for plant-available water (Glina et al., 2014; Paluszek, 2010; Rejman and Iglik, 2010) that is usually stored in the Bt horizons that are being actively eroded.

Short-term erosion rates, quantified using $^{239+240}$Pu fallout radionuclides (Loba et al., 2021), present an opportunity to speculate about the approximate timing of the disappearance of the Bt horizons (Table S2). Soil degradation seems to have been the most intense in WK2, WK8 and WK10, where the soil class may have significantly changed within ~ 200, 130 and 80 years, respectively. In these profiles, soil erosion was at its peak, already has led to a distinct shallowing of the loess mantle. In the other profiles, the prognosis seems to be slightly better, with the Bt horizon possibly having disappeared after 300 years. However, it needs to be borne in mind that these calculations are based on values calculated in the present day. Progressive climate change, causing soil drying and less frequent, but more intense, rainfall events, may lead to an increase in erosive events (Routschek et al., 2014; Zádorová and Penížek, 2018; Zollinger et al., 2015). Therefore, the disappearance of Luvisols may be even more accelerated. Thus, the effective application of anti-erosive treatments and sustainable land use is crucial to the protection of vital soil resources.

5. Conclusions

The luminescence (OSL) dating enabled to reconstruction time intervals of denudation processes in the studied loess area. In total, five soil redeposition phases took place starting from 9.1 ka. Other phases occurred ca. 6.4 ka, 3.8 ka, 1.5–0.7 ka and 0.4 ka. Due to the progressive denudation processes, the soil cover in the study area was very dynamic. Most likely, at the beginning of the Holocene, soils bearing chernic/mollic horizons developed in the loess mantle, which later, as a result of erosional/depositional processes, transformed into Luvisols. Modern soil erosion rates increased considerably, causing the removal of the eluvial and argic horizons, thus transforming the Luvisols into Regosols. This soil degradation causes a shallowing of the loess mantle, depletion in organic matter and nutrients and a reduction in crop productivity. Based on soil erosion rates, we calculate that the soil class may significantly change within ~ 80–300 years, although progressive climate change may intensify the erosion events, thus further accelerating the disappearance of the fertile loess mantle and Luvisols. Therefore, it is necessary to apply effective anti-erosion treatments, making landowners aware of the risks caused by erosion and thus implementing the European Parliament resolution on soil protection.

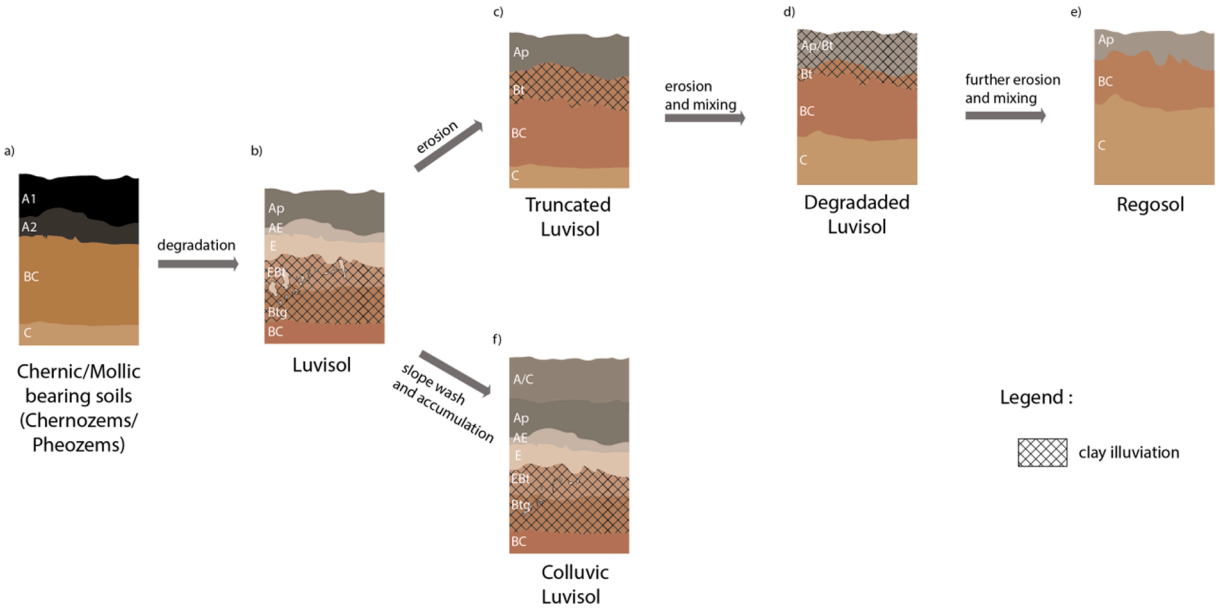

Fig. 8. Hypothetical pathways of soil evolution resulting from denudation processes in loess areas in Central Europe. (The model starts from the Chernozem/Pheozem predominating in the European loess belt during Late Glacial/early Holocene as showed by Labaz et al. (2018) and Kabała et al. (2019).

Uncited references

CRediT authorship contribution statement

Aleksandra Loba: Formal analysis, Visualization, Writing – original draft. **Junjie Zhang:** Writing – review & editing. **Sumiko Tsukamoto:** Writing – review & editing. **Marek Kasprzak:** Writing – review & editing. **Joanna Beata Kowalska:** Writing – review & editing. **Manfred Frechen:** Writing – review & editing. **Jarosław Waroszewski:** Conceptualization, Visualization, Writing – original draft, Project administration, Funding acquisition.

Declaration of Competing Interest

The authors declare that they have no known competing financial interests or personal relationships that could have appeared to influence the work reported in this paper.

Data availability

Data will be made available on request.

Acknowledgements

The authors are grateful to Krzysztof Papuga and Paweł Jezierski for their help during the fieldwork, to Sonja Riemenschneider and Sabine Mogwitz for support during laboratory analyses as well as to Marcin Sykuła for graphic support.

Funding

This research was financed by the National Science Center (Poland) project number 2018/29/B/ST10/01282 (Opus 15).

Appendix A. Supplementary data

Supplementary data to this article can be found online at https://doi.org/10.1016/j.catena.2022.106724.

References

Alewell, C., Pitois, A., Meusburger, K., Ketterer, M., Mabit, L., 2017. 239+240 Pu from "contaminant" to soil erosion tracer: Where do we stand? Earth-Science Rev. 172, 107–123. https://doi.org/10.1016/j.earscirev.2017.07.009.

Altermann, M., Rinklebe, J., Merbach, I., Körschens, M., Langer, U., Hofmann, B., 2005. Chernozem - Soil of the Year 2005. J. Plant Nutr. Soil Sci. 168, 725–740. https://doi.org/10.1002/jpln.200521814.

Anioł-Kwiatkowska, J., 1998. Endangered and rare segetal species in the microregion Trzebnica Hills. Acta Univ. Lodz. 13, 169–176.

Auclair, M., Lamothe, M., Huot, S., 2003. Measurement of anomalous fading for feldspar IRSL using SAR. Radiat. Meas. 37, 487–492. https://doi.org/10.1016/S1350-4487(03)00018-0.

Bac, S., Rojek, M., 2012. Meteorologia i klimatologia w inżynierii środowiska. Wydawnictwo Uniwersytetu Przyrodniczego we Wrocławiu, Wrocław.

Baumgart, P., Eltner, A., Domula, A.R., Barkleit, A., Faust, D., 2017. Scale dependent soil erosion dynamics in a fragile loess landscape. Zeitschrift für Geomorphol. 61 (3), 191–206.

Bronk Ramsey, C., 2009. Dealing with Outliers and Offsets in Radiocarbon Dating. Radiocarbon 51, 1023–1045. https://doi.org/10.1017/S0033822200034093.

Bronk Ramsey, C., 2001. Development of the Radiocarbon Calibration Program. Radiocarbon 43, 355–363. https://doi.org/10.1017/S0033822200038212.

Buylaert, J.-P., Jain, M., Murray, A.S., Thomsen, K.J., Thiel, C., Sohbati, R., 2012. A robust feldspar luminescence dating method for Middle and Late Pleistocene sediments. Boreas 41, 435–451. https://doi.org/10.1111/j.1502-3885.2012.00248.x.

Buylaert, J.-P., Thiel, C., Murray, A., Vandenberghe, D., Yi, S., Lu, H., 2011. IRSL and post-IR IRSL residual doses recorded in modern dust samples from the Chinese Loess Plateau. Geochronometria 38, 432–440. https://doi.org/10.2478/s13386-011-0047-0.

Chen, Y., Li, S.-H., Li, B., 2013. Residual doses and sensitivity change of post IR IRSL signals from potassium feldspar under different bleaching conditions. Geochronometria 40, 229–238. https://doi.org/10.2478/s13386-013-0128-3.

Döhler, S., Damm, B., Terhorst, B., Thiel, C., Frechen, M., 2015. Late Pleistocene and Holocene landscape formation in a gully catchment area in Northern Hesse. Germany. Quat. Int. 365, 42–59. https://doi.org/10.1016/j.quaint.2014.08.001.

Döhler, S., Terhorst, B., Frechen, M., Zhang, J., Damm, B., 2018. Chronostratigraphic interpretation of intermediate layer formation cycles based on OSL-dates from intercalated slope wash sediments. Catena 162, 278–290. https://doi.org/10.1016/j.catena.2017.11.003.

Dotterweich, M., 2008. The history of soil erosion and fluvial deposits in small catchments of central Europe: Deciphering the long-term interaction between humans and the environment — A review. Geomorphology 101, 192–208. https://doi.org/10.1016/j.geomorph.2008.05.023.

Dotterweich, M., Rodzik, J., Zgłobicki, W., Schmitt, A., Schmidtchen, G., Bork, H.-R., 2012. High resolution gully erosion and sedimentation processes, and land use changes since the Bronze Age and future trajectories in the Kazimierz Dolny area (Nałęczów Plateau, SE-Poland). CATENA 95, 50–62. https://doi.org/10.1016/j.catena.2012.03.001.

Dotterweich, M., Stankoviansky, M., Minár, J., Koco, Š., Papčo, P., 2013. Human induced soil erosion and gully system development in the Late Holocene and future perspectives on landscape evolution: The Myjava Hill Land, Slovakia. Geomorphology 201, 227–245. https://doi.org/10.1016/j.geomorph.2013.06.023.

Dreibrodt, S., Bork, H., 2021. Soil Erosion and Sedimentation in Central Europe From the Neolithic to the Industrial Revolution-The German and Polish Records. In: Reference Module in Earth Systems and Environmental Sciences. Elsevier, pp. 1–15. https://doi.org/10.1016/B978-0-12-818234-5.00061-4.

Dreibrodt, S., Hofmann, R., Dal Corso, M., Bork, H.-R., Duttmann, R., Martini, S., Saggau, P., Schwark, L., Shatilo, L., Videiko, M., Nadeau, M.-J., Grootes, P.M., Kirleis, W., Müller, J., 2022. Earthworms, Darwin and prehistoric agriculture-Chernozem genesis reconsidered. Geoderma 409, 115607. https://doi.org/10.1016/j.geoderma.2021.115607.

Dreibrodt, S., Jarecki, H., Lubos, C., Khamnueva, S.V., Klamm, M., Bork, H.-R., 2013. Holocene soil formation and soil erosion at a slope beneath the Neolithic earthwork Salzmünde (Saxony-Anhalt, Germany). CATENA 107, 1–14. https://doi.org/10.1016/j.catena.2013.03.002.

Dreibrodt, S., Lomax, J., Nelle, O., Lubos, C., Fischer, P., Mitusov, A., Reiss, S., Radtke, U., Nadeau, M., Grootes, P.M., Bork, H.-R., 2010a. Are mid-latitude slopes sensitive to climatic oscillations? Implications from an Early Holocene sequence of slope deposits and buried soils from eastern Germany. Geomorphology 122, 351–369. https://doi.org/10.1016/j.geomorph.2010.05.015.

Dreibrodt, S., Lubos, C., Terhorst, B., Damm, B., Bork, H.-R., 2010b. Historical soil erosion by water in Germany: Scales and archives, chronology, research perspectives. Quat. Int. 222, 80–95. https://doi.org/10.1016/j.quaint.2009.06.014.

Drewnik, M., Skiba, M., Szymański, W., Zyła, M., 2014. Mineral composition vs. soil forming processes in loess soils - A case study from Kraków (Southern Poland). Catena 119, 166–173. https://doi.org/10.1016/j.catena.2014.02.012.

Drewnik, M., Żyła, M., 2019. Properties and classification of heavily eroded post-chernozem soils in Proszowice Plateau (southern Poland). Soil Sci. Annu. 70, 225–233. https://doi.org/10.2478/ssa-2019-0020.

Dudek, M., Łabaz, B., Bednik, M., Medyńska-Juraszek, A., 2022. Humic Substances as Indicator of Degradation Rate of Chernozems in South-Eastern Poland. Agronomy 12, 733. https://doi.org/10.3390/agronomy12030733.

Duller, G.A.T., 2003. Distinguishing quartz and feldspar in single grain luminescence measurements. Radiat. Meas. 37, 161–165. https://doi.org/10.1016/S1350-4487(02)00170-1.

Eckmeier, E., Gerlach, R., Gehrt, E., Schmidt, M.W.I., 2007. Pedogenesis of Chernozems in Central Europe — A review. Geoderma 139, 288–299. https://doi.org/10.1016/j.geoderma.2007.01.009.

European Parliament, 2021. Resolution on soil protection (2021/2548(RSP)) [WWW Document]. URL https://www.europarl.europa.eu/doceo/document/TA-9-2021-0143_EN.html.

FAO, 2019. Soil erosion: the greatest challenge to sustainble soil management. Rome. https://doi.org/10.1080/00050326.1941.10437468.

FAO, 2006. Guidlines for soil description, 4th ed. Rome. https://doi.org/10.1007/978-3-030-33443-7_3.

Frechen, M., 2003. Loess in Europe—mass accumulation rates during the Last Glacial Period. Quat. Sci. Rev. 22, 1835–1857. https://doi.org/10.1016/S0277-3791(03)00183-5.

Fuchs, M., Fischer, M., Reverman, R., 2010. Colluvial and alluvial sediment archives temporally resolved by OSL dating: Implications for reconstructing soil erosion. Quat. Geochronol. 5, 269–273. https://doi.org/10.1016/j.quageo.2009.01.006.

Gerlach, R., Fischer, P., Eckmeier, E., Hilgers, A., 2012. Buried dark soil horizons and archaeological features in the Neolithic settlement region of the Lower Rhine area, NW Germany: Formation, geochemistry and chronostratigraphy. Quat. Int. 265, 191–204. https://doi.org/10.1016/j.quaint.2011.10.007.

Gillijns, K., Poesen, J., Deckers, J., 2005. On the characteristics and origin of closed depressions in loess-derived soils in Europe—a case study from central Belgium. CATENA 60, 43–58. https://doi.org/10.1016/j.catena.2004.10.001.

Glina, B., Waroszewski, J., Kabal, C., 2014. Water retention of the loess-derived Luvisols with lamellic illuvial horizon in the Trzebnica Hills (SW Poland). Soil Sci. Annu. 65, 18–24. https://doi.org/10.2478/ssa-2014-0003.

Godfrey-Smith, D.I., Huntley, D.J., Chen, W.-H., 1988. Optical dating studies of quartz and feldspar sediment extracts. Quat. Sci. Rev. 7, 373–380. https://doi.org/10.1016/0277-3791(88)90032-7.

Haase, D., Fink, J., Haase, G., Ruske, R., Pécsi, M., Richter, H., Altermann, M., Jäger, K. D., 2007. Loess in Europe-its spatial distribution based on a European Loess Map, scale 1:2,500,000. Quat. Sci. Rev. 26, 1301–1312. https://doi.org/10.1016/j.quascirev.2007.02.003.

Huntley, D.J., Lamothe, M., 2001. Ubiquity of anomalous fading in K-feldspars and the measurement and correction for it in optical dating. Can. J. Earth Sci. 38, 1093–1106. https://doi.org/10.1139/e01-013.
IUSS Working Group WRB, 2022. World Reference Base for Soil Resources. International soil classification system for naming soils and creating legends for maps, 4th edition. FAO, Rome, Vienna, Austria.
Jagercikova, M., Cornu, S., Bourlès, D., Antoine, P., Mayor, M., Guillou, V., 2015. Understanding long-term soil processes using meteoric 10Be: A first attempt on loessic deposits. Quat. Geochronol. 27, 11–21. https://doi.org/10.1016/j.quageo.2014.12.003.
Jagercikova, M., Evrard, O., Balesdent, J., Lefèvre, I., Cornu, S., 2014. Modeling the migration of fallout radionuclides to quantify the contemporary transfer of fine particles in Luvisol profiles under different land uses and farming practices. Soil Tillage Res. 140, 82–97. https://doi.org/10.1016/j.still.2014.02.013.
Jakab, G., Hegyi, I., Fullen, M., Szabó, J., Zacháry, D., Szalai, Z., 2018. A 300-year record of sedimentation in a small tilled catena in Hungary based on δ13C, δ15N, and C/N distribution. J. Soils Sediments 18, 1767–1779. https://doi.org/10.1007/s11368-017-1908-9.
Jarašiūnas, G., Świtoniak, M., Kinderienė, I., 2020. Dynamics of slope processes under changing land use conditions in young morainic landscapes. Western Lithuania. Int. Agrophysics 1, 43–55. https://doi.org/10.31545/intagr/116404.
Jary, Z., 1996. Chronostratygrafia oraz warunki sedymentacji lessów południowo-zachodniej Polski na przykładzie Płaskowyżu Głubczyckiego i Wzgórz Trzebnickich. Studia Geograficzne LXIII Uniwersytetu Wrocławskiego, Wrocław.pdf.
Kabała, C., Przybył, A., Krupski, M., Łabaz, B., Waroszewski, J., 2019. Origin, age and transformation of Chernozems in northern Central Europe – New data from Neolithic earthen barrows in SW Poland. Catena 180, 83–102. https://doi.org/10.1016/j.catena.2019.04.014.
Kaiser, K., Tolksdorf, J.F., de Boer, A.M., Herbig, C., Hieke, F., Kasprzak, M., Kočár, P., Petr, L., Schubert, M., Schröder, F., Fülling, A., Hemker, C., 2021. Colluvial sediments originating from past land-use activities in the Erzgebirge Mountains, Central Europe: occurrence, properties, and historic environmental implications. Archaeol. Anthropol. Sci. 13, 220. https://doi.org/10.1007/s12520-021-01469-z.
Karasiewicz, M.T., Hulisz, P., Świtoniak, M., 2014. Wpływ procesów denudacji na właściwości osadów wypełniających zagłębienia między krętymi wałami z erozji wód subglacjalnych w okolicy Zbójna (Pojezierze Dobrzyńskie). Landf. Anal. 25, 29–42. https://doi.org/10.12657/landfana.025.004.
Kars, R.H., Reimann, T., Wallinga, J., 2014. Are feldspar SAR protocols appropriate for post-IR IRSL dating? Quat. Geochronol. 22, 126–136. https://doi.org/10.1016/j.quageo.2014.04.001.
Kasprzak, M., Traczyk, A., 2014. LiDAR and 2D Electrical Resistivity Tomography as a Supplement of Geomorphological Investigations in Urban Areas: A Case Study from the City of Wrocław (SW Poland). Pure Appl. Geophys. 171, 835–855. https://doi.org/10.1007/s00024-013-0693-7.
Khokhlova, O.S., Chendev, Y.G., Myakshina, T.N., Alexandrovskiy, A.L., Khokhlov, A.A., 2015. Evolution of Chernozems in the southern forest-steppe of the Central Russian upland under long-term cultivation examined in the agro-chronosequences. Quat. Int. 365, 175–189. https://doi.org/10.1016/j.quaint.2014.10.012.
Klimowicz, Z., Uziak, S., 2001. The influence of long-term cultivation on soil properties and patterns in an undulating terrain in Poland. Catena 43, 177–189. https://doi.org/10.1016/S0341-8162(00)00162-4.
Kołodyńska-Gawrysiak, R., Chodorowski, J., Mroczek, P., Plak, A., Zgłobicki, W., Kiebała, A., Trzciński, J., Standzikowski, K., 2017. The impact of natural and anthropogenic processes on the evolution of closed depressions in loess areas. A multi-proxy case study from Nałęczów Plateau. Eastern Poland. CATENA 149, 1–18. https://doi.org/10.1016/j.catena.2016.07.029.
Kołodyńska-Gawrysiak, R., Poesen, J., Gawrysiak, L., 2018. Assessment of long-term Holocene soil erosion rates in Polish loess areas using sedimentary archives from closed depressions. Earth Surf. Process. Landforms 43, 978–1000. https://doi.org/10.1002/esp.4296.
Kopittke, P.M., Menzies, N.W., Wang, P., McKenna, B.A., Lombi, E., 2019. Soil and the intensification of agriculture for global food security. Environ. Int. 132, 105078 https://doi.org/10.1016/j.envint.2019.105078.
Krekelbergh, N., Frankl, A., Dondeyne, S., 2020. Understanding soil profiles and sediment redistribution over long time scales in an agrarian setting : the case of Lauwerdal (Northern France). EGU Gen. Assem. 2020. https://doi.org/10.5194/egusphere-egu2020-14026.
Kreutzer, S., Schmidt, C., Fuchs, M.C., Dietze, M., Fischer, M., Fuchs, M., 2012. Introducing an R package for luminescence dating analysis. Anc. TL 30, 1–8.
Krzyszkowski, D., Łabno, A., 2002. Late Saalian (Wartanian) glacial palaeogeography and formation of end moraines at the northern slope of Silesian Rampart, Southwestern Poland. Ann. Soc. Geol. Pol. 72, 67–87.
Kundzewicz, Z.W., Matczak, P., 2012. Climate change regional review: Poland. Wiley Interdiscip. Rev. Clim. Chang. 3, 297–311. https://doi.org/10.1002/wcc.175.
Labaz, B., Musztyfaga, E., Waroszewski, J., Bogacz, A., Jezierski, P., Kabala, C., 2018. Landscape-related transformation and differentiation of Chernozems – Catenary approach in the Silesian Lowland, SW Poland. Catena 161, 63–76. https://doi.org/10.1016/j.catena.2017.10.003.
Labaz, B., Waroszewski, J., Dudek, M., Bogacz, A., Kabala, C., 2022. Persistence of arable Chernozems and Chernic Rendzic Phaeozems in the eroded undulating loess plateau in Central Europe. CATENA 216, 106417. https://doi.org/10.1016/j.catena.2022.106417.
Łanczont, M., Komar, M., Madeyska, T., Mroczek, P., Standzikowski, K., Hołub, B., Fedorowicz, S., Sytnyk, O., Bogucki, A., Dmytruk, R., Yatsyshyn, A., Koropetskyi, R., Tomeniuk, O., 2021. Spatio-temporal variability of topoclimates and local palaeoenvironments in the Upper Dniester River Valley: Insights from the Middle and Upper Palaeolithic key-sites of the Halych region (western Ukraine). Quat. Int. 632, 112–131.
Lehmkuhl, F., Nett, J.J., Pötter, S., Schulte, P., Sprafke, T., Jary, Z., Antoine, P., Wacha, L., Wolf, D., Zerboni, A., Hošek, J., Marković, S.B., Obreht, I., Sümegi, P., Veres, D., Zeeden, C., Boemke, B., Schaubert, V., Viehweger, J., Hambach, U., 2021. Loess landscapes of Europe – Mapping, geomorphology, and zonal differentiation. Earth-Science Rev. 215, 103496 https://doi.org/10.1016/j.earscirev.2020.103496.
Leopold, M., Hürkamp, K., Völkel, J., Schmotz, K., 2011. Black soils, sediments and brown calcic luvisols: A pedological description of a newly discovered neolithic ring ditch system at Stephansposching, Eastern Bavaria. Germany. Quat. Int. 243, 293–304. https://doi.org/10.1016/j.quaint.2010.11.021.
Li, G., Wen, L., Xia, D., Duan, Y., Rao, Z., Madsen, D.B., Wei, H., Li, F., Jia, J., Chen, F., 2015. Quartz OSL and K-feldspar pIRIR dating of a loess/paleosol sequence from arid central Asia, Tianshan Mountains, NW China. Quat. Geochronol. 28, 40–53. https://doi.org/10.1016/j.quageo.2015.03.011.
Li, M., Li, Z., Liu, P., Yao, W., 2005. Using Cesium-137 technique to study the characteristics of different aspect of soil erosion in the Wind-water Erosion Crisscross Region on Loess Plateau of China. Appl. Radiat. Isot. 62, 109–113. https://doi.org/10.1016/j.apradiso.2004.06.005.
Liritzis, I., Stamoulis, K., Papachristodoulou, C., Ioannides, K., 2013. A re-evaluation of radiation dose-rate conversion factors. Mediterr. Archaeol. Archaeom. 13, 1–15.
Liu, C., Li, Z., Chang, X., He, J., Nie, X., Liu, L., Xiao, H., Wang, D., Peng, H., Zeng, G., 2018. Soil carbon and nitrogen sources and redistribution as affected by erosion and deposition processes: A case study in a loess hilly-gully catchment. China. Agric. Ecosyst. Environ. 253, 11–22. https://doi.org/10.1016/j.agee.2017.10.028.
Loba, A., Waroszewski, J., Sykuła, M., Kabala, C., Egli, M., 2022. Meteoric 10Be, 137Cs and 239+240Pu as Tracers of Long- and Medium-Term Soil Erosion—A Review. Minerals 12, 359. https://doi.org/10.3390/min12030359.
Loba, A., Waroszewski, J., Tikhomirov, D., Calitri, F., Christl, M., Sykuła, M., Egli, M., 2021. Tracing erosion rates in loess landscape of the Trzebnica Hills (Poland) over time using fallout and cosmogenic nuclides. J. Soils Sediments 21, 2952–2968. https://doi.org/10.1007/s11368-021-02996-x.
Malik, I., Poręba, G., Wistuba, M., Woskowicz-Ślęzak, B., 2021. Combining 137Cs, 210Pb and dendrochronology for improved reconstruction of erosion–sedimentation events in a loess gully system (southern Poland). L. Degrad. Dev. 32, 2336–2350. https://doi.org/10.1002/ldr.3903.
Matecka, P., Świtoniak, M., 2020. Delineation, characteristic and classification of soils containing carbonates in plow horizons within young moraine areas. Soil Sci. Annu. 71, 23–36. https://doi.org/10.37501/soilsa/121489.
Meij, W.M., Reimann, T., Vornehm, V.K., Temme, A.J.A.M., Wallinga, J., Beek, R., Sommer, M., 2019. Reconstructing rates and patterns of colluvial soil redistribution in agrarian (hummocky) landscapes. Earth Surf. Process. Landforms 44, 2408–2422. https://doi.org/10.1002/esp.4671.
Morgan, R.P., 2005. Soil erosion and conservation. Blackwell Science Ltd.
Moska, P., Jary, Z., Adamiec, G., Bluszcz, A., 2019. Chronostratigraphy of a loess-palaeosol sequence in Biały Kościół, Poland using OSL and radiocarbon dating. Quat. Int. 502, 4–17. https://doi.org/10.1016/j.quaint.2018.05.024.
Muhs, D.R., 2013. The geologic records of dust in the quaternary. Aeolian Res. 9, 3–48. https://doi.org/10.1016/j.aeolia.2012.08.001.
Murray, A.S., Thomsen, K.J., Masuda, N., Buylaert, J.P., Jain, M., 2012. Identifying well-bleached quartz using the different bleaching rates of quartz and feldspar luminescence signals. Radiat. Meas. 47, 688–695. https://doi.org/10.1016/j.radmeas.2012.05.006.
Nachtergaele, J., Poesen, J., 2002. Spatial and temporal variations in resistance of loess-derived soils to ephemeral gully erosion. Eur. J. Soil Sci. 53, 449–463. https://doi.org/10.1046/j.1365-2389.2002.00443.x.
Novák, T.J., Molnár, M., Buró, B., 2018. Reconstruction of Soil Carbon Redistribution Processes along a Hillslope Section in a Forested Area. Radiocarbon 60, 1413–1424. https://doi.org/10.1017/RDC.2018.94.
Olley, J.M., Roberts, R.G., Murray, A.S., 1997. Disequilibria in the uranium decay series in sedimentary deposits at Allen's cave, nullarbor plain, Australia: Implications for dose rate determinations. Radiat. Meas. 27, 433–443. https://doi.org/10.1016/S1350-4487(96)00114-X.
Paluszek, J., 2013. Assessment of soil structure of Luvisols developed from loess classified in various complexes of agricultural suitability. Soil Sci. Annu. 64, 41–48. https://doi.org/10.2478/ssa-2013-0008.
Paluszek, J., 2010. Zmiany pokrywy glebowej pod wpływem erozji. Pr. i Stud. Geogr. 45, 279–294.
Pindral, S., Świtoniak, M., 2017. The usefulness of soil-agricultural maps to identify classes of soil truncation. Soil Sci. Annu. 68, 2–10. https://doi.org/10.1515/ssa-2017-0001.
Poręba, G., Śnieszko, Z., Moska, P., 2011. Some aspects of age assessment of Holocene loess colluvium: OSL and 137Cs dating of sediment from Biała agricultural area, South Poland. Quat. Int. 240, 44–51. https://doi.org/10.1016/j.quaint.2011.02.005.
Poręba, G., Śnieszko, Z., Moska, P., Mroczek, P., Malik, I., 2019. Interpretation of soil erosion in a Polish loess area using OSL, 137Cs, 210Pbex, dendrochronology and micromorphology – case study: Biedrzykowice site (s Poland). Geochronometria 46, 57–78. https://doi.org/10.1515/geochr-2015-0109.
Poręba, G.J., Śnieszko, Z., Moska, P., 2015. Application of OSL dating and 137Cs measurements to reconstruct the history of water erosion: A case study of a Holocene colluvium in Świerklany, south Poland. Quat. Int. 374, 189–197. https://doi.org/10.1016/j.quaint.2015.04.004.
Prescott, J.R., Hutton, J.T., 1994. Cosmic ray contributions to dose rates for luminescence and ESR dating: Large depths and long-term time variations. Radiat. Meas. 23, 497–500. https://doi.org/10.1016/1350-4487(94)90086-8.

Qin, J., Chen, J., Li, Y., Zhou, L., 2018. Initial sensitivity change of K-feldspar pIRIR signals due to uncompensated decrease in electron trapping probability: Evidence from radiofluorescence measurements. Radiat. Meas. 120, 131–136. https://doi.org/10.1016/j.radmeas.2018.06.017.

Raab, G., Martin, A.P., Norton, K.P., Christl, M., Scarciglia, F., Egli, M., 2021. Complex patterns of schist tor exposure and surface uplift, Otago (New Zealand). Geomorphology 389, 107849. https://doi.org/10.1016/j.geomorph.2021.107849.

Raab, G., Scarciglia, F., Norton, K., Dahms, D., Brandová, D., Castro Portes, R., Christl, M., Ketterer, M.E., Ruppli, A., Egli, M., 2018. Denudation variability of the Sila Massif upland (Italy) from decades to millennia using 10Be and 239+240Pu. L. Degrad. Dev. 29, 3736–3752. https://doi.org/10.1002/ldr.3120.

Radziuk, H., Świtoniak, M., 2021. Soil erodibility factor (K) in soils under varying stages of truncation. Soil Sci. Annu. 72, 1–8. https://doi.org/10.37501/soilsa/134621.

Rahimzadeh, N., Khormali, F., Gribenski, N., Tsukamoto, S., Kehl, M., Pint, A., Kiani, F., Frechen, M., 2019. Timing and development of sand dunes in the Golestan Province, northern Iran—Implications for the Late-Pleistocene history of the Caspian Sea. Aeolian Res. 41, 100538 https://doi.org/10.1016/j.aeolia.2019.07.004.

Rees-Jones, J., Tite, M.S., 1997. Optical dating results for British archaeological sediments. Archaeometry 39, 177–187. https://doi.org/10.1111/j.1475-4754.1997.tb00797.x.

Reimann, T., Tsukamoto, S., Naumann, M., Frechen, M., 2011. The potential of using K-rich feldspars for optical dating of young coastal sediments – A test case from Darss-Zingst peninsula (southern Baltic Sea coast). Quat. Geochronol. 6, 207–222. https://doi.org/10.1016/j.quageo.2010.10.001.

Reimer, P.J., Bard, E., Bayliss, A., Beck, J.W., Blackwell, P.G., Ramsey, C.B., Buck, C.E., Cheng, H., Edwards, R.L., Friedrich, M., Grootes, P.M., Guilderson, T.P., Haflidason, H., Hajdas, I., Hatté, C., Heaton, T.J., Hoffmann, D.L., Hogg, A.G., Hughen, K.A., Kaiser, K.F., Kromer, B., Manning, S.W., Niu, M., Reimer, R.W., Richards, D.A., Scott, E.M., Southon, J.R., Staff, R.A., Turney, C.S.M., van der Plicht, J., 2013. IntCal13 and Marine13 Radiocarbon Age Calibration Curves 0–50,000 Years cal BP. Radiocarbon 55, 1869–1887. https://doi.org/10.2458/azu_js_rc.55.16947.

Rejman, J., Iglik, I., 2010. Topsoil reduction and cereal yields on loess soils of southeast Poland. L. Degrad. Dev. 21, 401–405. https://doi.org/10.1002/ldr.963.

Rejman, J., Iglik, I., Paluszek, J., Rodzik, J., 2014a. Soil redistribution and crop productivity in loess areas (Lublin Upland, Poland). Soil Tillage Res. 143, 77–84. https://doi.org/10.1016/j.still.2014.05.011.

Rejman, J., Rafalska-Przysucha, A., Rodzik, J., 2014b. The Effect of Land Use Change on Transformation of Relief and Modification of Soils in Undulating Loess Area of East Poland. Sci. World J. 2014, 1–11. https://doi.org/10.1155/2014/341804.

Rejman, J., Rodzik, J., 2006. Soil erosion in Europe -. In: Boardman, J., Poesen, J. (Eds.), Soil Erosion in Europe. John Wiley & Sons Ltd, Poland, pp. 95–106.

Reynolds, J.M., 2011. Electrical Resistivity Method, in: An Introduction to Applied and Environmental Geophysics. Willey, pp. 289–372.

Rommens, T., Verstraeten, G., Lang, A., Poesen, J., Govers, G., Van Rompaey, A., Lang, A., Peeters, I., 2005. Soil erosion and sediment deposition in the Belgian oess belt during the Holocene: establishing a sediment budget for a small agricultural catchment. The Holocene 15, 1032–1043. https://doi.org/10.1191/0959683605hl876ra.

Routschek, A., Schmidt, J., Kreienkamp, F., 2014. Impact of climate change on soil erosion - A high-resolution projection on catchment scale until 2100 in Saxony/Germany. Catena 121, 99–109. https://doi.org/10.1016/j.catena.2014.04.019.

Scheib, A.J., Birke, M., Dinelli, E., 2014. Geochemical evidence of aeolian deposits in European soils. Boreas 43 (1), 175–192.

Scherer, S., Deckers, K., Dietel, J., Fuchs, M., Henkner, J., Höpfer, B., Junge, A., Kandeler, E., Lehndorff, E., Leinweber, P., Lomax, J., Miera, J., Poll, C., Toffolo, M. B., Knopf, T., Scholten, T., Kühn, P., 2021. What's in a colluvial deposit? Perspectives from archaeopedology. Catena 198, 105040.

Šimanský, V., Juriga, M., Mendyk, Ł., 2019. Slope position and management practices as factors influencing selected properties of topsoil. Soil Sci. Annu. 70, 137–146. https://doi.org/10.2478/ssa-2019-0012.

Smetanová, A., Verstraeten, G., Notebaert, B., Dotterweich, M., Létal, A., 2017. Landform transformation and long-term sediment budget for a Chernozem-dominated lowland agricultural catchment. CATENA 157, 24–34. https://doi.org/10.1016/j.catena.2017.05.007.

Starkel, L., 2005. Role of climatic and anthropogenic factors accelerating soil erosion and fluvial activity in Central Europe. Stud. Quat. 22, 27–33.

Starkel, L., Michczyńska, D.J., Krąpiec, M., Margielewski, W., Nalepka, D., Pazdur, A., 2013. Progress in the holocene chrono-climatostratigraphy of Polish territory. Geochronometria 40, 1–21. https://doi.org/10.2478/s13386-012-0024-2.

Stoops, G., 2003. Guidlines for analysis and description of soil and regolith thin section/. Soil Science Society of America Inc, Madison, Wisconsin, USA.

Strouhalová, B., Gebhardt, A., Ertlen, D., Šefrna, L., Flašarová, K., Kolařík, P., Schwartz, D., 2020. From Chernozem to Luvisol or from Luvisol to Chernozem? A discussion about the relationships and limits of the two types of soils. A case study of the soil catena of Hrušov. Czechia. Geografie 125, 473–500. https://doi.org/10.37040/geografie2020125040473.

Świtoniak, M., Mroczek, P., Bednarek, R., 2016. Luvisols or Cambisols? Micromorphological study of soil truncation in young morainic landscapes - Case study: Brodnica and Chełmno Lake Districts (North Poland). Catena 137, 583–595. https://doi.org/10.1016/j.catena.2014.09.005.

Terhorst, B., 2000. The influence of Pleistocene landforms on soil-forming processes and soil distribution in a loess landscape of Baden-Württemberg (south-west Germany). CATENA 41, 165–179. https://doi.org/10.1016/S0341-8162(00)00098-9.

Thomsen, K.J., Murray, A.S., Jain, M., Bøtter-Jensen, L., 2008. Laboratory fading rates of various luminescence signals from feldspar-rich sediment extracts. Radiat. Meas. 43, 1474–1486. https://doi.org/10.1016/j.radmeas.2008.06.002.

Tuo, D., Xu, M., Gao, G., 2018. Relative contributions of wind and water erosion to total soil loss and its effect on soil properties in sloping croplands of the Chinese Loess Plateau. Sci. Total Environ. 633, 1032–1040. https://doi.org/10.1016/j.scitotenv.2018.03.237.

Turski, M., Witkowska-Walczak, B., 2004. Fizyczne właściwości gleb płowych wytworzonych z utworów pyłowych różnej genezy (in Polish). Acta Agrophysica 101.

Van Oost, K., Govers, G., Van Muysen, W., 2003. A process-based conversion model for caesium-137 derived erosion rates on agricultural land: an integrated spatial approach. Earth Surf. Process. Landforms 28, 187–207. https://doi.org/10.1002/esp.446.

Vitharana, U.W.A., Van Meirvenne, M., Simpson, D., Cockx, L., De Baerdemaeker, J., 2008. Key soil and topographic properties to delineate potential management classes for precision agriculture in the European loess area. Geoderma 143, 206–215. https://doi.org/10.1016/j.geoderma.2007.11.003.

Wacha, K.M., Thanos Papanicolaou, A.N., Giannopoulos, C.P., Abban, B.K., Wilson, C.G., Zhou, S., Hatfield, J.L., Filley, T.R., Hou, T., 2018. The role of hydraulic connectivity and management on soil aggregate size and stability in the clear creek watershed. Iowa. Geosci. 8, 1–18. https://doi.org/10.3390/geosciences8120470.

Wallinga, J., 2002. Optically stimulated luminescence dating of fluvial deposits: a review. Boreas 31, 303–322. https://doi.org/10.1080/030094802320942536.

Wallinga, J., Murray, A., Duller, G., 2000. Underestimation of equivalent dose in single-aliquot optical dating of feldspars caused by preheating. Radiat. Meas. 32, 691–695. https://doi.org/10.1016/S1350-4487(00)00127-X.

Waroszewski, J., Pietranik, A., Sprafke, T., Kabała, C., Frechen, M., Jary, Z., Kot, A., Tsukamoto, S., Meyer-Heintze, S., Krawczyk, M., Łabaz, B., Schultz, B., Erban Kochergina, Y.V., 2021. Provenance and paleoenvironmental context of the Late Pleistocene thin aeolian silt mantles in south-west Poland – a widespread parent material for soils. Catena 204. https://doi.org/10.1016/j.catena.2021.105377.

Winnicki, J., 1997. Geological structure of the Trzebnica Hills in the light of new investigation. Geol. Q. 41, 365–380.

Winnicki, J., 1990. Objaśnienia do Szczegółowej Mapy Geologicznej Polski 1:50 000, Arkusz Trzebnica (727).

Winnicki, J., 1985. Szczegółowa Mapa Geologiczna Polski 1:50 000, Arkusz Trzebnica (727).

Wintle, A.G., Murray, A.S., 2006. A review of quartz optically stimulated luminescence characteristics and their relevance in single-aliquot regeneration dating protocols. Radiat. Meas. 41, 369–391. https://doi.org/10.1016/j.radmeas.2005.11.001.

Yu, K., Xu, H., Lan, J., Sheng, E., Liu, B., Wu, H., Tan, L., Yeager, K.M., 2017. Climate change and soil erosion in a small alpine lake basin on the Loess Plateau. China. Earth Surf. Process. Landforms 42, 1238–1247. https://doi.org/10.1002/esp.4071.

Zádorová, T., Penížek, V., 2018. Formation, morphology and classification of colluvial soils: a review. Eur. J. Soil Sci. 69, 577–591. https://doi.org/10.1111/ejss.12673.

Zádorová, T., Penížek, V., Šefrna, L., Drábek, O., Mihaljevič, M., Volf, Š., Chuman, T., 2013. Identification of Neolithic to Modern erosion–sedimentation phases using geochemical approach in a loess covered sub-catchment of South Moravia, Czech Republic. Geoderma 195–196, 56–69. https://doi.org/10.1016/j.geoderma.2012.11.012.

Zádorová, T., Penížek, V., Šefrna, L., Rohošková, M., Borůvka, L., 2011. Spatial delineation of organic carbon-rich Colluvial soils in Chernozem regions by Terrain analysis and fuzzy classification. Catena 85, 22–33. https://doi.org/10.1016/j.catena.2010.11.006.

Zádorová, T., Žížala, D., Penížek, V., Čejková, Š., 2014. Relating extent of colluvial soils to topographic derivatives and soil variables in a luvisol sub-catchment, Central Bohemia. Czech Republic. Soil Water Res. 9, 47–57. https://doi.org/10.17221/57/2013-swr.

Zgłobicki, W., Rodzik, J., 2007. Heavy metals in the slope deposits of loess areas of the Lublin Upland (E Poland). Catena 71, 84–95. https://doi.org/10.1016/j.catena.2006.10.008.

Zhang, J., 2018. Behavior of the electron trapping probability change in IRSL dating of K-feldspar: A dose recovery study. Quat. Geochronol. 44, 38–46. https://doi.org/10.1016/j.quageo.2017.12.001.

Zhang, J., Yang, M., Sun, X., Zhang, F., 2018a. Estimation of wind and water erosion based on slope aspects in the crisscross region of the Chinese Loess Plateau. J. Soils Sediments 18, 1620–1631. https://doi.org/10.1007/s11368-017-1855-5.

Zhang, K., Pan, S., Liu, Z., Li, G., Xu, Y., Hao, Y., 2018b. Vertical distributions and source identification of the radionuclides 239Pu and 240Pu in the sediments of the Liao River estuary. China. J. Environ. Radioact. 181, 78–84. https://doi.org/10.1016/j.jenvrad.2017.10.016.

Zhang, W., Xing, S., Hou, X., 2019. Evaluation of soil erosion and ecological rehabilitation in Loess Plateau region in Northwest China using plutonium isotopes. Soil Tillage Res. 191, 162–170. https://doi.org/10.1016/j.still.2019.04.004.

Zollinger, B., Alewell, C., Kneisel, C., Meusburger, K., Brandová, D., Kubik, P., Schaller, M., Ketterer, M., Egli, M., 2015. The effect of permafrost on time-split soil erosion using radionuclides (137Cs, 239 + 240Pu, meteoric 10Be) and stable isotopes (δ13C) in the eastern Swiss Alps. J. Soils Sediments 15, 1400–1419. https://doi.org/10.1007/s11368-014-0881-9.